Russian Chemical Reviews **73** (9) 861 – 880 (2004) © 2004 Russian Academy of Sciences and Turpion Ltd

DOI 10.1070/RC2004v073n09ABEH000919

The role of heteroepitaxy in the development of new thin-film oxide-based functional materials

A R Kaul, O Yu Gorbenko, A A Kamenev

Contents

I.	Introduction	861
II.	Epitaxial stabilisation	861
III.	Variant structures	874
IV.	Conclusion	878

Abstract. The methods of synthesis of new oxide compounds and thin-film materials based on the use of heteroepitaxy are considered. The thermodynamic model and the theory of the epitaxial stabilisation phenomenon are outlined, the role of thermodynamic and structure-geometric factors determining the possibility of epitaxial stabilisation of unstable phases is interpreted. The use of epitaxial stabilisation for the design of heterostructures with specific electric properties is demonstrated. The characteristic features of the structural relations between the film and substrate materials, resulting in the formation of thin films with different numbers of variants, are discussed. The bibliography includes 128 references.

I. Introduction

Epitaxy, *i.e.*, oriented growth of a crystal on another crystal, has long been used to synthesise thin-film materials. This is the simplest and the most economical way of preparing structurally perfect film materials, which successfully replace single crystals with large diameters. Numerous examples of using epitaxial processes in elementary semiconductors are known, in particular, heteroepitaxy of silicon films on the surface of a sapphire single crystal, preparation of films of the Si_xGe_{1-x} solid solution on the surface of single crystal silicon plates, silicon autoepitaxy on silicon plates and so on. By means of epitaxy, one can produce materials with different widths of the forbidden gap. The most impressive results in the design of semiconductor materials of the $A^{III}B^{V}$ family for optoelectronics were attained using this method. Epitaxy was used to obtain layers with a low concentration of defects and periodic structures with alternation of numerous layers with diverse compositions several nanometers thick. For the synthesis of such structures, a MOC-hydride process has been developed and special highly automated equipment has been designed (in particular, AIXTRON equipment has found extensive application).

A R Kaul, O Yu Gorbenko Department of Chemistry, M V Lomonosov Moscow State University, Leninskie Gory, 119992 Moscow, Russian Federation. Fax (7-095) 939 14 92. Tel. (7-095) 939 14 92.
E-mail: kaul@inorg.chem.msu.ru (A R Kaul),
gorbenko@inorg.chem.msu.ru (O Yu Gorbenko)
A A Kamenev YUKOS Research and Development Centre, Leninsky prosp. 55/1, Building 2, 119333 Moscow, Russian Federation.
Fax (7-095) 730 61 02. Tel. (7-095) 730 61 01 (2-26)

Received 9 March 2004
Uspekhi Khimii **73** (9) 932 – 953 (2004); translated by Z P Bobkova

Unlike the epitaxy of semiconductors, the epitaxy of oxides is far from being well-developed in both theoretical and engineering aspects, although the demand for oxide materials in semiconductor engineering was realised long ago. This lag is due to a number of reasons, most of all, to the great diversity of structures and chemical properties of oxides. It often remains unknown whether it is possible to perform epitaxial intergrowth of oxides corresponding to different structural types and having different lattice parameters. The necessity of using high temperature and, most often, a high partial pressure of oxygen promotes side chemical reactions of oxides, in particular, those with the products of surface oxidation of semiconductors. These circumstances appreciably complicate the preparation of epitaxial oxide materials. In addition, the structural and chemical diversity of oxides accounts for more diverse manifestations of the epitaxy (compared to those for semiconductors) and opens up new prospects for the application of this phenomenon.

This review deals with two original methods for the preparation of new thin-film oxide materials, namely, epitaxial stabilisation of unstable phases and the design of variant structures. The review mainly presents the studies carried out by researchers engaged in the chemistry and physics of thin oxide films at the Chair of Inorganic Chemistry of the Department of Chemistry of the M V Lomonosov Moscow State University.

II. Epitaxial stabilisation

1. The principles of epitaxial stabilisation

The last 15 years have seen intensive research into the preparation of epitaxial films of multicomponent complex oxides. The attention of researchers was focused on perovskite-type or related compounds, which possess unique properties. These include high temperature semiconductors of the $RBa_2Cu_3O_{7-\delta}$ (R is lanthanide) and Bi – Ca – Sr – Cu – O families, the $Pb(Ti,Zr)O_3$ and $(Ba,Sr)TiO_3$ ferroelectrics, materials with colossal magnetoresistance $La_{1-x}(Ca,Sr)_xMnO_3$, and electron – ion conductors $La_{1-x}(Sr,Ca)_xCoO_3$.

Much effort was devoted to methods for the preparation of multicomponent oxide films, such as metal organic chemical vapour deposition (MOCVD), pulse laser deposition (PLD), magnetron sputtering, *etc*. Despite the difference, these methods have one feature in common — the mass transfer processes that underlie them are incongruent, *i.e.*, during the substance transfer from the target or the gas phase onto the substrate, the ratio of the cationic components changes to some extent. This often violates the stoichiometry of the cationic composition of the films and usually gives rise to second phases (inclusions). In order to obtain single-phase epitaxial films, the composition of the target or the

flow of volatile components should be consistently corrected based on the results of elemental analysis of films.

Examination of phase analysis data for off-stoichiometric epitaxial films has shown that impurity phases often differ from those expected relying on the known phase diagrams of the systems under consideration. In addition, it was found that the growth of single-phase epitaxial films often takes place under thermodynamic conditions (P_{O_2} and T) where this compound as a bulk material (polycrystalline powder, ceramics or a single crystal) is thermodynamically unstable. These phenomena are of a common nature and can be explained by phase stabilisation due to the epitaxy on the substrate or due to the epitaxy at the interface between two phases formed simultaneously (the matrix and the inclusion).

The relationship between the formation of metastable phases and the epitaxy was first noted by Dankov [1,2] when growing oxide layers on metals. Later, van der Merwe [3,4] performed a comprehensive theoretical analysis of the growth of epitaxial layers. The data they obtained were summarised to formulate the structural and size compliance principle (the Dankov–van der Merwe principle). As applied to epitaxial stabilisation, this principle can be outlined as follows: the competitive formation of new phases on a substrate surface would predominantly yield phases congruent to the substrate. In Russian publications, this is called more often the Dankov–Konobeevskii principle.

The appearance of metastable phases on the single crystal surface may be of both thermodynamic and kinetic nature. The Dankov–van der Merwe principle is apparently applicable both to systems in which the particle diffusion in the growing layer is sufficient for ensuring a phase equilibrium and to systems in which diffusion is retarded.

In the systems we are interested in, epitaxial films of complex oxides grow, most often, at high temperatures ($\sim 600-900\,^{\circ}C$), *i.e.*, the thermodynamic factor predominates. Depending on the structural correspondence between the film and the substrate, either epitaxial or polycrystalline films are formed. Experiments show that the phase composition of the polycrystalline films does not differ from that predicted by equilibrium phase diagrams for the given elemental composition and the number of phases obeys the Gibbs phase rule. In addition, the phase composition is reproduced in successive experiments on film preparation and does not change during long-term annealing at the film deposition temperature. These findings prove that the polycrystalline oxide layers formed on the substrates in the above-indicated temperature range are quite close to true thermodynamic equilibrium,† although film growth from the gas phase is undoubtedly a non-equilibrium process.

As regards epitaxial films produced under the same conditions, their phase composition is also reproducible and also does change after long-term annealing at the temperature of film growth. However, the phase composition of the epitaxial films, unlike that of polycrystalline films, often does not correspond to that predicted relying on the equilibrium phase diagram. However, epitaxial films are much closer to an ideal single crystal and have a lower free energy than polycrystalline films of the identical composition, as they do not have an extensive internal surface typical of polycrystals. Thus, one can state that the observed deviations of the phase composition of the oxide epitaxial films from that predicted on the basis of equilibrium phase diagrams constructed for bulk states are due to thermodynamic factors. These deviations are related to the formation of new equilibrium phase relations in the film material. This is caused by the decrease in the system free energy following a decrease in the contribution of the free energy of the film/substrate interface in the case where they are structurally coherent.

The epitaxial stabilisation (ES) can be defined, from the thermodynamic standpoint, as extension of the $P-T-x$ space of the thermodynamically stable existence of the epitaxial phase with respect to the bulk state of this phase free from a substrate.

Table 1 presents examples of epitaxial stabilisation which shows itself as metamorphism of simple and complex oxides, the formation of new oxide phase and as the stabilisation of compounds containing metals in unstable oxidation states.

This Table is not meant to be exhaustive, giving only the epitaxial phases formed upon epitaxial stabilisation of the thermodynamic origin. It is noteworthy that most of the researchers cited were prone to treat the results they obtained as a curiosity observed for unknown reasons in a particular system rather than a predictable phenomenon of the thermodynamic nature.

In the next Sections, we consider the theoretical foundations of the epitaxial stabilisation and demonstrate, using our studies as examples, that this phenomenon can be utilised for the synthesis of new solid-state compounds and new materials.

The greater part of the data included in Table 1 refer to the polymorphism of simple oxides. This is due to several reasons: first, the preparation of the phases of simple oxides is not complicated by the necessity of controlling the cationic composition; second, selection of the $P_{O_2}-T$ conditions for their synthesis is more obvious than in other cases; third, highly symmetric single-crystal substrates can be used in their synthesis.

Examples of preparing new compounds with complex compositions due to the ES are scarce since the necessary conditions unknown in advance, namely, the stochiometric ratio of the cations, the $P_{O_2}-T$ film growth conditions, and the similarity of growing film and substrate parameters, are unlikely to be simultaneously fulfilled by chance. The choice of these conditions should be deliberate.

2. The thermodynamic model of epitaxial stabilisation

Let us consider the formation of a new phase nucleus on the surface of a single crystal during deposition from the gas phase. The Gibbs energy (ΔG_f) of the formation of this nucleus‡ is described by the equation:

$$\Delta G_f = \Delta g_V V + \sigma S + \Delta G^{El}, \quad (1)$$

where Δg_V is the specific volume Gibbs energy, J m^{-3}; σ is the surface tension, N m^{-1}; V and S are the volume and the surface area of the nucleus, respectively; ΔG^{El} is the contribution of elastic tension arising in the nucleus due to the compressive or tension effect of the substrate. Note the difference between the units of measurement of the free Gibbs energy (ΔG_f) and the specific volume Gibbs energy (Δg_V), the former being related to one nucleus of the phase and expressed in J and the latter being related to the unit volume of the phase and measured in J m^{-3}. The Δg_V value can be determined directly from the standard thermodynamic parameters, while ΔG_f is calculated from Eqn (1) and takes into account the energetic contributions of the volume and the surface of the nucleus and stress in the nucleus. For a thermodynamically stable phase, $\Delta g_V < 0$, while the energy contribution of the nucleus surface to the Gibbs energy is always positive ($\sigma S > 0$), which hampers the growth of the nucleus.

Now we consider in more detail the contributions of all components to ΔG_f using the Little and Zangwill formalism.[49]

To simplify the manipulation, we will make a number of model assumptions which do not influence the results. We consider the influence of epitaxy on the growth of an oxide film in which a polymorphic transition of the $A' \rightarrow A''$ type, where A' is a phase coherent to the substrate and A'' is a non-coherent phase, may take place. For conservation of the amount of substance, as a first approximation, one can neglect the difference between the densities ρ of the two competing polymorphic forms A' and A''.

† This statement implies impossibility of further solid-state transformations in the layer.

‡ The calculation of the free energy of formation of a nucleus is a routine procedure in consideration of nucleation thermodynamics.[48]

Table 1. Epitaxial stabilisation of oxide phases in thin films.

Epitaxially stabilised phases (structural type)	Substrate [a] [misfit of the unit cell parameters of the film and the substrate $(a_f - a_s)/a_s$]	Equilibrium phases formed in bulk materials under the same conditions (structural type)	Film thickness /nm	Film deposition method	Remarks	Ref.
Metamorphism						
Simple oxides						
TiO_2 (anatase)	(001)$SrTiO_3$ (−3.1%)	TiO_2 (rutile)	1000	MOCVD, molecular beam epitaxy (MBE)	deposition on the leucosapphire (Al_2O_3) with different orientation on the surface under the same conditions gives rutile	5–9
	(001)$LaAlO_3$ (−0.2%)	TiO_2 (rutile)	$n \times 10$	MBE		10
	$La_{0.5}Sr_{0.5}CoO_3$ (−0.5%)	TiO_2 (rutile)	–	PLD		11
	(001)MgO (−10.1%)	TiO_2 (rutile)	1000	MOCVD		6
	(110)MgO (−10.1%, 12.9%)	TiO_2 (rutile)	1000	MOCVD		6
ZnO (sphalerite)	ZnS/(001)GaAs	ZnO (wurtzite)	560	MBE from organometallic compounds		12
Mn_3O_4 (cubic spinel)	(001)MgO	Mn_3O_4 (hausmannite, tetragonal spinel)	–	MOCVD		13
WO_3 (tetragonal phase)	*R*-Al_2O_3 (10.3%, 2.5%)	WO_3 (orthorhombic phase)	30	electron beam evaporation		14
γ-Fe_2O_3	(001)MgO (−0.9%)	α-Fe_2O_3	100	MBE	deposition on the leucosapphire (*a*-, *c*- and *R*-Al_2O_3) under the same conditions gives α-Fe_2O_3	15
Complex oxides						
$BaRuO_3$ (perovskite)	(001)$SrTiO_3$	$BaRuO_3$ (hexagonal, 9R)	100	radio frequency sputtering		16, 17
$Sr(Ru_{0.5}Sn_{0.5})O_3$ (perovskite)	(001)$KTaO_3$ (0.25%)	$Sr(Ru_{0.5}Sn_{0.5})O_3$ (hexagonal, 4H or 9R)	600	PLD		18
$BaTi_{1-x}Nb_xO_3$ (x = 0.01–0.15) (hexagonal)	*R*-Al_2O_3 (17%)	$BaTi_{1-x}Nb_xO_3$ (x = 0.01–0.15) (perovskite)	60	PLD	deposition on (001)$SrTiO_3$ gives perovskite	19
β-BaB_2O_4	*c*-Al_2O_3, *R*-Al_2O_3	α-BaB_2O_4	–	PLD	deposition on (001)Si gives α-BaB_2O_4	20
$PbZr_{1-x}Ti_xO_3$ (pyrochlore)	(001)CeO_2/*R*-Al_2O_3 (3.8%)	$PbZr_{1-x}Ti_xO_3$ (perovskite)	–	PLD	deposition on (001)$SrTiO_3$ and (001)LiF gives perovskite	21
Epitaxial stabilisation of new oxide phases						
Complex oxides						
$Bi_3Fe_5O_{12}$ (garnet)	(001)$Gd_3(Sc,Ga)_5O_{12}$, (111)$Gd_3(Sc,Ga)_5O_{12}$ (<0.5%)	$BiFeO_3$ + $Bi_2Fe_4O_9$	<1000	reaction deposition from ion beams		22, 23
				plasma sputtering, radio frequency sputtering		24, 25
				PLD		22, 26, 27
Ba_2RuO_4 (K_2NiF_4 type)	(001)$SrTiO_3$ (2.1%)	no data	150	PLD	no Ba_2RuO_4 phase is formed on the substrates: (001)MgO, (001)$MgAl_2O_4$, (001)$LaSrGaO_4$, (001)$LaAlO_3$, (001)$LaAlO_3$–Sr_2AlTaO_6	28
Epitaxial stabilisation of oxide phases with metal atoms in unusual oxidation states						
Simple oxides						
CrO_2 (rutile)	TiO_2 (rutile) in different orientations (2%–4%), *c*-Al_2O_3 (−7.1%, 6.0 %)	Cr_2O_3 (corundum)	1000	MOCVD	$T \leqslant 550$ °C, P_{O_2} = 1 bar, CrO_2 is not formed on SiO_2 (quartz)	29–35

Table 1 (continued).

Epitaxially stabilised phases (structural type)	Substrate [a] [misfit of the unit cell parameters of the film and the substrate $(a_f - a_s)/a_s$]	Equilibrium phases formed in bulk materials under the same conditions (structural type)	Film thickness /nm	Film deposition method	Remarks	Ref.
Epitaxial stabilisation of oxide phases with metal atoms in unusual oxidation states						
Simple oxides						
MnO (NaCl type)	c-Al_2O_3, (111)MgO	Mn_3O_4	500	PLD	T = 700 °C, P_{O_2} = $= 10^{-4}$ mbar	36
Fe_3O_4 (spinel)	(001)MgO (0.4%)	Fe_2O_3 (corundum)	–	MBE	corundum grows on c-Al_2O_3	37–39
Fe_3O_4 (spinel)	(001)MgO (0.4%)	Fe	–	MBE	Fe grows on c-Al_2O_3	37–39
$Fe_{3-\delta}O_4$ ($0 < \delta < 0.33$) (spinel)	(001)MgO (0.4%–0.8%)	Fe_2O_3 (corundum)	–	MBE	corundum grows on c-Al_2O_3	15, 37–46
$Fe_{1-x}O$ (NaCl type)	(001)MgO (2.3%)	Fe + Fe_3O_4	–	MBE	T = 450 °C	45
Complex oxides						
$LaCuO_{3-\delta}$ (δ = 0.5) (orthorhombic phase)	(001)$SrTiO_3$ (−2.3%, −0.6%)	$LaCuO_{3-\delta}$ ($0.2 < \delta < 0.5$) (monoclinic phase)	300	PLD	T = 650–750 °C, P_{O_2} = 0.26 mbar	47

[a] The orientations of the perovskite substrates are given in the cubic system.

This assumption does not introduce a significant error but eliminates the necessity of knowing the density or the molar volume (V'_M) of the coherent phase in the absence of stresses (in particular, the latter value is difficult to estimate for a material obtained only as a stressed film).

Assume that new-phase nuclei having a square base with side d and height h are formed on the surface of a single-crystalline substrate representing a two-dimensional lattice with a square unit cell. The relative misfit of the crystal lattice parameters of the substrate and the film at the interface will be defined as

$$\varepsilon = (a_f - a_s)/a_s = \Delta a/a_s ,$$

where a_f and a_s are the unit cell parameters of the growing film and the surface, respectively. Let us consider the case where the film occurs in a uniformly strained state. The expressions for calculating the Gibbs energies for the formation of unit nuclei of the coherent ($\Delta G'_f$) and non-coherent phases ($\Delta G''_f$) can be written as

$$\Delta G'_f = \Delta g'_V d^2 h + (\sigma^s_c)' d^2 + (\sigma^V)'(d^2 + 4dh) + h\frac{\mu}{1-\nu}\varepsilon^2 d^2, \quad (2)$$

$$\Delta G''_f = \Delta g''_V d 2h + (\sigma^s_{ic})'' d^2 + (\sigma^V)''(d^2 + 4dh). \quad (3)$$

The subscripts c and ic refer to the coherent and non-coherent states of the interface, respectively, and the superscripts s and V refer to the nucleus / substrate and nucleus / surrounding gas phase interfaces, respectively. The last term in Eqn (2) is the contribution of the epitaxial stress energy of the nucleus of the coherent phase. This includes the shear modulus μ and Poisson's ratio ν.

The nucleus of the non-coherent phase A″ occurs in a relaxed (*i.e.*, unstressed) state, because it is not bound epitaxially to the substrate. Therefore, Eqn (3) does not have a term corresponding to the stress energy in the nucleus. It is worth mentioning that the surface tension at the non-coherent nucleus/substrate interface is much higher than at the coherent nucleus/substrate interface, $(\sigma^s)' \ll (\sigma^s)''$. The surface tensions at the interfaces between A′ and A″ and the surrounding vapour phase can be taken to be equal: $(\sigma^V)' = (\sigma^V)''$.

We will assume that the non-coherent phase A″, which is free from the substrate, is thermodynamically more stable than the coherent phase A′ under the $P_{O_2} - T$ conditions of film preparation, *i.e.*,

$$\Delta g''_V < \Delta g'_V .$$

[On the substrate, the relative stability of the phases may change due to the pronounced differences between $(\sigma^s)'$ and $(\sigma^s)''$.] By subtracting Eqn (2) from Eqn (3), we get the expression for the Gibbs energy that characterises the stability of one polymorphic form with respect to the other one. Dividing both equations into d^2 (for simplification) gives the equation for determining the Gibbs energy of unit surface of the nucleus ($\Delta E_f = \Delta G_f/d^2$). Hence,

$$\Delta E = \Delta E''_f - \Delta E'_f = \quad (4)$$
$$= h\left[(\Delta g''_V - \Delta g'_V) - \frac{\mu}{1-\nu}\varepsilon^2\right] + \left[(\sigma^s_{ic})'' - (\sigma^s_c)'\right].$$

To take into account the difference between the densities of phases A′ and A″, the difference $(\Delta g''_V - \Delta g'_V)$ should be replaced by

$$\frac{\Delta g''_V V''_M - \Delta g'_V V'_M}{V'_M} = \frac{\Delta G_t}{V'_M},$$

where ΔG_t is the free energy of the solid-state transition per mole.

Equation (4) reflects the opposite effects of two contributions to the Gibbs energy, the surface and the volume ones. Indeed, the first term (the total contribution of the volume energy) is always negative, whereas the second term (the total contribution of the surface energy and the epitaxial stress) is always positive. If the ratio of these contributions is such that $\Delta E > 0$, the condition of epitaxial stabilisation of the coherent phase A′ is fulfilled, although in the free state, this phase is less stable than the non-coherent phase A″. Thus, the ΔE value is the energy of epitaxial stabilisation.

As can be seen from Eqn (4), the misfit between the unit cell parameters of the phase being stabilised and the substrate is a highly significant parameter. The dependence of ΔE on the misfit parameter ε follows a quadratic law, whereas the dependences on the difference between the specific Gibbs energies and the difference between the interface energies with the substrate are linear. The variation of the ES *vs.* film thickness is also linear. The equilibrium condition for the two polymorphic forms A′ and A″ ($\Delta E = 0$) is met at a critical film thickness (h_c):

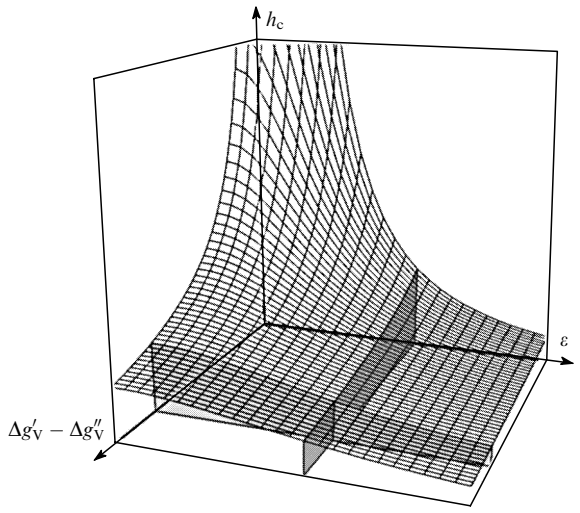


Figure 1. Critical film thickness (h_c) *vs.* the misfit of the unit cell parameters at the substrate/epitaxial film interface (ε) and *vs.* the difference between the specific volume energies of the unstable and stable phases.

$$h_c = \frac{(\sigma^s_{ic})'' - (\sigma^s_c)'}{(\Delta g'_V - \Delta g''_V) + [\mu/(1-\nu)]\varepsilon^2}. \quad (5)$$

Figure 1 shows a draft view of the dependence of the critical film thickness on the misfit of the cell parameters at the film/substrate interface and on the difference between the specific volume energies of the stable and unstable phases.

When the difference between specific volume energies of the competing polymorphic forms and the misfit between the cell parameters of the substrate and the stabilised form are small, the critical film thickness may be fairly large. Estimation of the h_c value from Eqn (5) shows that for a difference between the free energies of the phases of ~ 10 kJ mol^{-1} (this value is usual for polymorphic forms at a moderate deviation of the thermodynamic conditions from the polymorphic transition point), $\varepsilon \approx 0.01$ and for interfacial energies taken from published sources (presented below, see Ref. 50), the critical thickness of the stabilised layer amounts to tens of nanometres.

Interface (i)	Coherent (c)	Semicoherent (sc)	Non-coherent (ic)
σ^s_i /mJ m^{-2}	5–200	200–800	800–2500

When the film thickness is about several tens of nanometres, the model of uniformly strained film is no longer realistic. Stress relaxation in a non-uniformly strained film occurs through the formation of misfit dislocations. In this case, Eqn (4) should be supplemented by a term taking into account the non-uniformity of stresses. For simplicity, we assume that the Burgers vector of the misfit dislocation is equal to the unit cell parameter of the film a_f. Then the expression for ΔE has the form

$$\Delta E = h\left[(\Delta g''_V - \Delta g'_V) - \frac{\mu}{1-\nu}\left(\varepsilon - \frac{a_f}{l}\right)^2\right] + \quad (6)$$
$$+\left[(\sigma^s_{ic})'' - (\sigma^s_c)'\right] - \frac{1}{l}\left[E_{core} + \frac{\mu}{1-\nu}Ka_f^2 \exp\left(-\frac{4\pi h}{l}\right)\right],$$

where l is the distance between the neighbouring misfit dislocations, E_{core} is the energy of the dislocation nucleus and K is the pre-exponential factor. In the limit, $l = a_f/\varepsilon$, which corresponds to full relaxation of the epitaxial stress and disappearance of the term taking into account the contribution of uniform stresses from Eqn (6). When $h > a_f/\varepsilon$, the exponential term in the expression for non-uniform stress also disappears and the remaining addend, which does not depend on the film thickness, can be introduced as a correction for the interfacial energy [this correction transforms the energy of a coherent interface (σ_c) into the energy of a semicoherent interface (σ_{sc})]:

$$\Delta E = h(\Delta g''_V - \Delta g'_V) + [(\sigma^s_{ic})'' - (\sigma^s_{sc})']. \quad (7)$$

The term $[(\sigma^s_{ic})'' - (\sigma^s_{sc})']$ in Eqn (7) is positive, while the term depending on the film thickness is negative. The contribution of the surface energy $[(\sigma^s_{ic})'' - (\sigma^s_{sc})']$ to the Gibbs energy is lower in the case of a non-uniformly strained film than for a uniformly strained film with a coherent interface due to the higher energy of the semicoherent interface. However, the first (positive, 'destabilising') term also decreases in this case due to disappearance of the stress contribution. Thus, the epitaxial stabilisation can also take place in the growth of relaxed films on semicoherent substrates. In other words, epitaxial stresses in the film are not obligatory for the epitaxial stabilisation. Taking the difference between the Gibbs energies of the polymorphic forms to be, as in the previous case, 10 kJ mol^{-1} and substituting the interfacial energies into Eqn (7), one can estimate the critical thickness of the stabilised phase. The result is of the order of tens of nanometres.

The experience in preparation of thin films indicates that the phase non-coherent to the substrate always grows as a polycrystal. The internal interfaces in a polycrystalline materials make a substantial contribution to the Gibbs energy. This contribution (so-called excessive Gibbs energy), which has not yet been included in the energy balance of two polymorphic phases, undoubtedly affects the epitaxial stabilisation. Assuming that the average grain size in the non-coherent phase equals r and the average energy of the boundaries of chaotically oriented grains equals σ''_{gb} and taking into account the fact that the number of grains on unit surface equals d^2/r^2 ($d \gg r$), we obtain a relation for the total energy of the grain boundaries of the non-coherent phase concentrated on unit surface area of the substrate

$$E_{gb} = \frac{2h\,\sigma''_{gb}}{r}. \quad (8)$$

By substituting the E_{gb} value as an additional term for the non-coherent phase energy, into Eqn (7), we get an expression for the epitaxial stabilisation energy

$$\Delta E = h\left[(\Delta g''_V - \Delta g'_V) + \frac{2\,\sigma''_{gb}}{r}\right] + [(\sigma^s_{ic})'' - (\sigma^s_{sc})']. \quad (9)$$

It should be noted that the surface tension σ''_{gb} in a polycrystalline film is of the same order of magnitude as σ_{ic}, and, hence, the influence of polycrystallinity, which increases ΔE, may become prevailing. The role of this factor appreciably increases with a decrease in the grain size. As the polycrystalline film of the stable phase grows, the grain size does not remain constant but increases; however, under steady-state conditions of growth, this increase follows the law $r \propto \sqrt[n]{h}$ ($n \geqslant 2$). Therefore, the increase in the grain size does not much decrease the excessive free energy of the intergrain boundaries and, finally, does not interfere with the preparation of the epitaxially stabilised phase as films with a large critical thickness.

In order to verify the applicability of Eqns (7) and (9) for the calculation of ΔE, we will consider the results of calculations of the polymorphic transition TiO_2(anatase) → TiO_2(rutile) (Fig. 2). It follows from the data of Table 1 that the TiO_2(anatase) film grows on the (001)$LaAlO_3$ surface epitaxially to form a semicoherent interface. According to the above data, the energy of the semicoherent interface between the thin film and the substrate can be taken to be $(\sigma^s_{sc})' = 800$ mJ m^{-2}. A hypothetical film of the stable rutile phase could grow in the polycrystalline form under these conditions. The energy of the non-coherent interface between such a film and a substrate $(\sigma^s_{ic})''$ can amount to 2500 mJ m^{-2}; the non-coherent intergrain boundaries σ''_{gb} have the same energy. The difference between the specific volume energies $(\Delta g''_V - \Delta g'_V)$ calculated using the published value of the Gibbs energy for the TiO_2(anatase) → TiO_2(rutile) transition (-5 kJ mol^{-1}) [51, 52] and

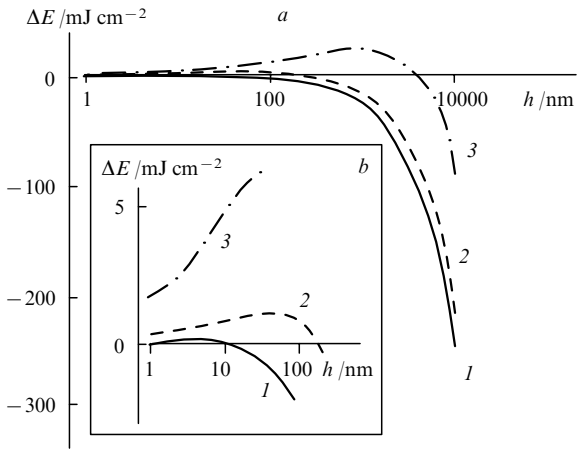


Figure 2. Results of model calculations for the TiO_2(anatase) → TiO_2(rutile) polymorphic transition using Eqns (7) (curve *1*) and (9) (curves *2* and *3*) (*a*). The inset (*b*) shows the enlarged view of the initial course of curves *1*–*3*;
r/μm: ∞ (*1*), 25 (*2*), 1 (*3*).

the theoretical density values for rutile and anatase (4.25 and 3.89 g cm^{-3}, respectively), is equal to 243.7 J cm^{-3}.

It can be seen from Fig. 2 that the anatase epitaxial film is thermodynamically more stable than the rutile polycrystalline film when the film thickness is smaller than the critical value h_c, corresponding to the condition $\Delta E = 0$. With the reasonable assumption that the rutile film can be formed by crystallites with the size $\sqrt{h}$, we finally get that the critical thickness of an epitaxially stabilised film of anatase can reach 4 μm! Although the exact value of h_c depends on the numerical values $(\sigma^s_{ic})''$, $(\sigma^s_{sc})''$ and σ''_{gb} used for calculations, this calculation still proves the theoretical possibility of preparing stabilised phases as epitaxial films with a sufficient thickness for many practical applications. In other words, the epitaxial stabilisation can be an efficient tool for the preparation of new functional materials.

Undoubtedly, crystallisation under real conditions is much more complicated than is described in terms of the above model. First of all, this model does not take into account any kinetic effects, resulting in accumulation of non-equilibrium point and extended defects in the epitaxial films (stacking faults, antiphase boundaries, development of mosaic block low-angle boundaries) and ultimately in the inevitable disappearance of the epitaxy following an increase in the film thickness. Apparently, these kinetic effects rather than the value we calculated from thermodynamic considerations are responsible for restriction of the stabilised phase thickness. Thus, the growth of films under conditions favourable for acceleration of diffusion processes and crystallisation, in particular, the growth at a temperature exceeding the Tamman temperature,§ or implementation of the liquid-phase growth mechanism (for example, vapour–liquid–crystal or the liquid-phase epitaxy) would promote the formation of stabilised phases as epitaxial films with the critical thickness predicted by the thermodynamic model outlined above.

This model can be applied not only to a polymorphic transformation of two phases but also to more complicated phase ensembles; however, considering such ensembles requires much more complicated equations but does not reveal any new significant aspects of epitaxial stabilisation.

§ The Tamman temperature is the temperature above which intensive self-diffusion occurs in a solid. As a rule, the Tamman temperature is taken to be 0.6 T_m (the Tamman rule).

3. Preparation of epitaxial oxide films by MOCVD

Metal organic chemical vapour deposition (MOCVD) is a promising and efficient method for the preparation of films of simple and complex oxides.

The MOCVD method has a number of obvious advantages over the high-vacuum physical (physical vapour deposition, PVD) methods, in particular,

— relatively low cost,
— relatively low requirements to the vacuum equipment,
— the possibility of high deposition rate,
— remarkable versatility as regards the variation of the elemental composition of films.

These advantages make the MOCVD method very attractive for the modern technology of films and coatings. A substantial progress in the development of this method as applied to the production of films of simple and complex oxides has been attained during the last 15 years. This was largely due to the advent of methods for the preparation of epitaxial films of high-temperature superconductors (HTSC), especially those of the $RBa_2Cu_3O_{7-\delta}$ family.[53] The superconducting properties of films are highly sensitive to minor changes in the composition and structure; therefore, the problem of preparing HTSC with reproducible properties is much more challenging than the problem of preparing other thin-film materials. The advances attained in MOCVD syntheses of HTSC films stimulated the extension of this method to many other functional oxide materials often having rather complex elemental composition.

The heterogeneous MOCVD process consists of several consecutive stages: evaporation or sublimation of the starting compounds (volatile organometallic compounds), their transfer through the gas phase (often complicated by gas-phase reactions) and, finally, oxidative thermolysis on the substrate with simultaneous crystallisation of the product. Each stage is complicated. In the case of multicomponent films, the difference between the chemical and thermal properties of compounds used to transport each of the starting components results in a substantial incongruence of the process, *i.e.*, in different stoichiometric ratios of the metallic components in the vapour of the starting compounds and in the film. This is the major syntetic challenge in the preparation of multicomponent films.[54, 55]

Nevertheless, the synthesis of new volatile compounds with improved properties (more stable and more volatile) for a large number of metals, perfection of batching and vaporisation techniques and the design of more advanced reactors with optimised thermal fields and gas dynamics turned MOCVD into an advanced process technology.

Most often, metal dipivaloylmethanates $M(dpm)_n$ or their adducts with *o*-phenanthroline were used as the starting compounds for the synthesis of the thin films of manganites $R_{1-x}M_xMnO_3$ (R = La–Lu; M = Ca, Sr, Pb, Na), nickelates $RNiO_3$ (R = La, Pr, Nd, Sm, Gd), cobaltates $RCoO_3$ (R = Tm, Lu), ferrites $RFeO_3$ (R = Eu–Lu), garnets $R_3Fe_5O_{12}$ (R = Nd, $Nd_{1-x}La_x$), indates $RInO_3$ (R = La–Lu), ruthenates $(Ca,Sr)RuO_3$ and superconductive cuprates $RBa_2Cu_3O_{7-\delta}$ (R = Lu, Ho, Y, Gd) considered in this review. These compounds were evaporated as microbatches fed successively to the evaporating chamber; thus, the flash vaporisation principle, which minimises the thermal degradation of the precursors, was implemented. Various special devices (feeders) were used for the supply of precursors: aerosol, vibratory, belt, frictional and screw feeders. The precursor vapours were transported by an argon–oxygen stream to tubular reactors heated by the external resistance furnace or induction method.

The temperature of the substrates (usually single crystals cut along a definite plane and polished) was varied, depending on the system, in the 650–900 °C range and the oxygen pressure was 1–7 mbar. The total pressure in the reactors (maintained constant in each experiment) was in the range 3–20 mbar. The

MOCVD conditions are described in more detail in our original publications.[53, 56–60]

4. Epitaxial stabilisation of unstable compounds RMO_3 (R is lanthanide, M = Mn, Ni, Co, Fe, In)

Manganites $RMnO_3$. In the series of $RMnO_3$, phases with the perovskite structure are formed under ambient pressure only for lanthanides with great ionic radii (R = La–Dy), whereas elements with smaller ionic radii (Y, Ho–Lu) form hexagonal structures with the same stoichiometry.[61] The corresponding perovskites $RMnO_3$ (Y, Ho–Lu) were prepared only under high pressure.[62] However, the situation can change upon the change in the contribution of the surface free energy. Thus the $YMnO_3$ nanoparticles synthesised under normal pressure are no longer hexagonal but have a perovskite structure.[63]

We attained epitaxial stabilisation of the perovskite phase $RMnO_3$ (R = Y, Ho, Tm, Lu) by MOCVD deposition of the $RMnO_3$ films onto the (001)$LaAlO_3$ and (001)$SrTiO_3$ substrates.[64] The orthorhombically distorted perovskite $YMnO_3$ was also prepared by PLD on a substrate.[65]

The most efficient stabilisation takes place on the $LaAlO_3$ substrate because this is characterised by a minimum misfit ($\sim$0.5%) between the unit cell parameters and the growing perovskite film. Using this substrate, 100–200-nm thick perovskite films were prepared (T = 750 °C). Under the same conditions, no perovskite phase is formed on the $(1\bar{1}02)Al_2O_3$ and (111)$ZrO_2(Y_2O_3)$ substrates. The resulting perovskite films were structurally identical to those formed in the polycrystalline state at high pressure: their perovskite structure experienced substantial orthorhombic distortion (orthorhombicity parameter $\sim$5%, space group *Pnma*). The distortion of the perovskite structure gave rise to twinning in the films. According to powder X-ray diffraction and high-resolution transmission electron microscopy (HREM) of film cross-sections, the unit cell parameters are always doubled along the substrate plane (Figs 3, 4) and the direction of doubling of the cell parameter in each successive domain is changed by 90°. This type of twinning reduces the stress arising in the film due to the misfit in the cell parameters of the film and the substrate because this markedly decreases the energy of the film/substrate interface, in conformity with the theory developed by Little and Zangwill.[49]

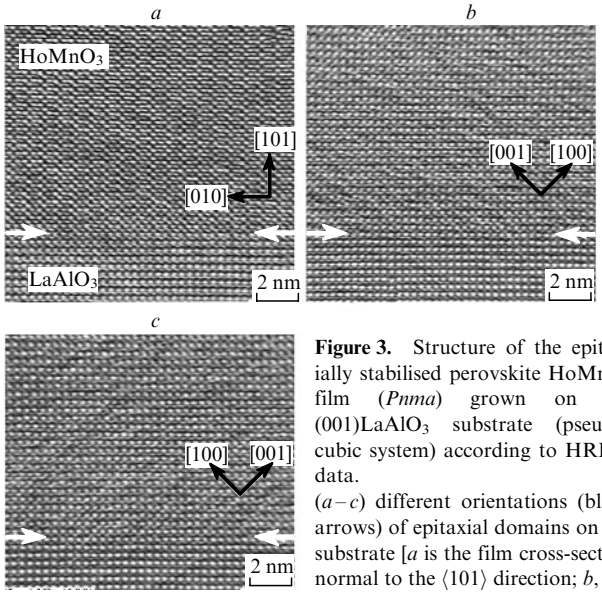


Figure 3. Structure of the epitaxially stabilised perovskite $HoMnO_3$ film (*Pnma*) grown on the (001)$LaAlO_3$ substrate (pseudocubic system) according to HREM data.
(*a*–*c*) different orientations (black arrows) of epitaxial domains on the substrate [*a* is the film cross-section normal to the ⟨101⟩ direction; *b*, *c* is the same normal to the ⟨010⟩ direction.] Here and below, light arrows designate the film/substrate boundary.

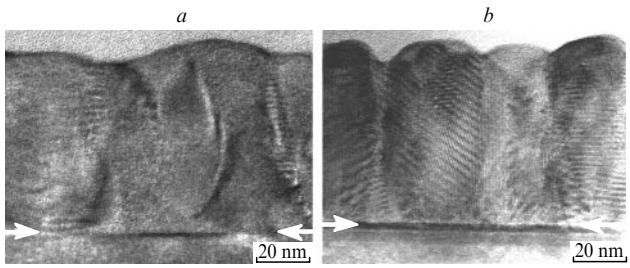


Figure 4. Photomicrograph of the cross-section of $HoMnO_3$ (*a*) and $LuMnO_3$ (*b*) perovskite films on the (001)$LaAlO_3$ substrate (TEM data).

The size of domains correlates with the misfit of the crystal lattice parameters between the film and the substrate at the interface; an increase in the misfit results in a decrease in the size of domains. For example, much more extended domains are formed in the perovskite $HoMnO_3$ films (Fig. 4*a*) than in $LuMnO_3$ films (Fig. 4*b*).

The results of investigations of the real structure of $RMnO_3$ perovskite films confirm the conclusion drawn above, namely, that a stress in the lattice is not a necessary factor of epitaxial stabilisation, as some researchers believe [see, for example, A Zunger, D Wood *J. Cryst. Growth* **98** 1 (1989)].

Compounds $RMnO_3$ with a hexagonal structure of the $LuMnO_3$ type (space group $P6_3cm$) stable under ambient pressure are formed only for lanthanide cations with small ionic radii (R = Ho–Lu, Y). Their structure can be represented as a close packing of oxygen ions (ABCACB) in which the Mn^{3+} ions occupy positions with C.N. 5 (a five-vertex trigonal bipyramid), while the R^{3+} ions occur in positions with C.N. 7 (a seven-fold one-cap octahedron).[57] The interest in these compounds is due to the fact that they crystallise in space group $P6_3cm$. It is known that compounds that belong to this structural type can exhibit ferroelectric properties. In particular, $YMnO_3$ is a promising ferroelectric, which could find application in electronics.[66]

The complex oxide $DyMnO_3$ ($r_{Dy} > r_{Ho}$), prepared under usual solid-state synthesis conditions, has a stable perovskite structure. For this compound to crystallise in the hexagonal phase, heat treatment at a temperature of $\geqslant$1600 °C with subsequent quenching is required.[63] The greater the lanthanide ionic radius, the higher the temperature of the perovskite-to-hexagonal phase transition. Indeed, for $GdMnO_3$, the temperature of this polymorphic transition should be as high as about 2800 °C (determined by extrapolation), which knowingly exceeds the melting point of this compound and other manganites. In other words, $RMnO_3$ with R = Gd and larger lanthanide ions cannot exist as stable bulk samples in a hexagonal modification; however, these can be obtained as thin films using epitaxial stabilisation.[67]

On the basis of the available structural data for stable hexagonal phases, (111)$ZrO_2(Y_2O_3)$ was concluded to be the substrate of choice for the synthesis of hexagonal epitaxial films. In this case, the crystallographic positions of oxygen atoms at the substrate/hexagonal $RMnO_3$ interface perfectly coincide and the misfit parameter ε is a minimum [the films deposited on the (001)$LaAlO_3$, (001)MgO and (001)$ZrO_2(Y_2O_3)$ substrates had purely perovskite structures]. The X-ray diffraction patterns of the $DyMnO_3$, $GdMnO_3$ and $EuMnO_3$ films on the (111)$ZrO_2(Y_2O_3)$ substrate (Fig. 5) contained both symmetric (00*l*) and asymmetric (111), (112) reflections typical of a hexagonal structure of the $LuMnO_3$ type (asymmetric reflections are not shown in Fig. 5). It should be noted that the intensity of the (00*l*) reflections from the hexagonal phase decreases on passing from Dy to Eu and becomes zero for Sm; conversely, the intensity of the perovskite reflections increases in the same sequence. This means that the $DyMnO_3$ film grows as a purely hexagonal phase, the $EuMnO_3$ and $GdMnO_3$ films contain the hexagonal phase coexisting with the perovskite one (this was confirmed by recording the

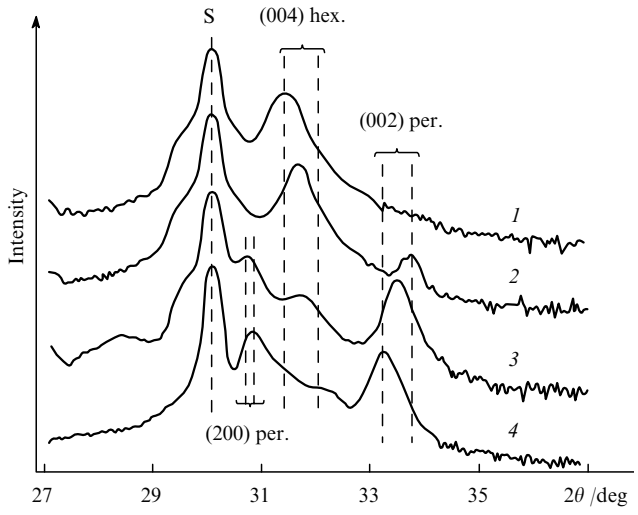


Figure 5. X-Ray diffraction patterns ($Cu_{K\alpha}$) of the $RMnO_3$ films grown on (111)$ZrO_2(Y_2O_3)$. R = Dy (*1*), Gd (*2*), Eu (*3*), Sm (*4*). Here and below, the reflections marked by S correspond to the substrate.

pole figures), and the $SmMnO_3$ film contains only the perovskite phase.

The hexagonal phase is *c*-oriented [as follows from X-ray φ-scanning spectra (Fig. 6) and pole figure images] and has the following epitaxial relations:

$$(001)_{hex}\,\langle 1\bar{1}0\rangle_{hex}\,RMnO_3 \parallel (111)\langle 1\bar{1}0\rangle\,ZrO_2(Y_2O_3),$$

i.e., the hexagonal (001) plane is parallel to the (111) plane of the substrate; the direction $\langle 1\bar{1}0\rangle_{hex}$ of $RMnO_3$ and $\langle 1\bar{1}0\rangle$ of the cubic substrate are also parallel.

Figure 7 shows the model of the epitaxial growth (polyhedral image) of the hexagonal $RMnO_3$ phase on (111)$ZrO_2(Y_2O_3)$.

It should be noted that an increase in the film thickness to 300 nm entailed an increase in the intensity only of perovskite reflections and not of reflections from the hexagonal phase. This indicates that the hexagonal phase grows only in the region adjacent to the substrate, while away from the substrate (in the upper part of the film), the usual perovskite phase is formed, stable in the bulk materials with this composition.

By extrapolating the available thermodynamic data on lanthanide manganites[68] to the region of epitaxially stabilised phases, one can estimate the thermodynamic effect of the ES for manganites with the perovskite and hexagonal structures (Fig. 8).

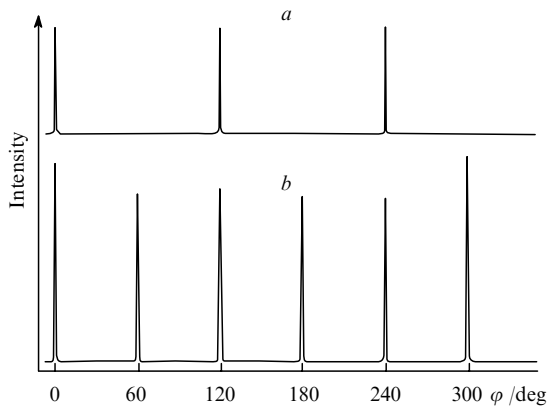


Figure 6. X-Ray diffraction spectra (φ-scanning) of the (111)$ZrO_2(Y_2O_3)$ substrate (*a*) and the $DyMnO_3$ film (*b*).
(*a*) {100}, χ = 55°, FWHM = 0.25°; (*b*) {112}, χ = 61°, FWHM = 0.55° (FWHM is the full width at half maximum, χ is the slope angle).

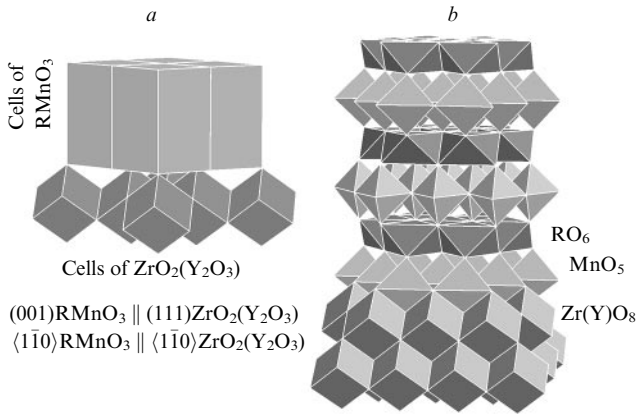


Figure 7. Model of the epitaxial growth of the $RMnO_3$ hexagonal phase on (111)$ZrO_2(Y_2O_3)$ (polyhedral image).
(*a*) Correlation of the substrate and film unit cells; (*b*) packing of the layers.

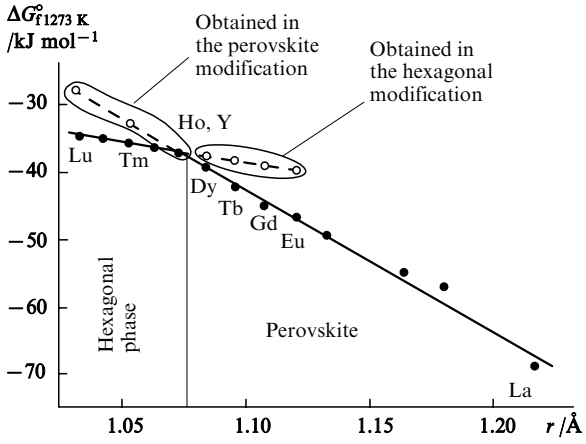


Figure 8. Gibbs energy of the formation of $RMnO_3$ (R is lanthanide) by the reactions $1/2\,R_2O_3 + 1/3\,Mn_3O_4 + 1/12\,O_2 = RMnO_3$ *vs.* ionic radius of the lanthanide (from Ref. 68).
The dashed lines represent the extrapolation to the epitaxial stabilisation region.

It can be stated that the ES of a thermodynamically less stable phase is possible if the difference between the Gibbs energies of the formation of the polymorphic forms does not exceed 10–15 kJ mol^{-1}, because in this case, the difference between the Gibbs energies can be counterbalanced by the decrease in the free energy of the system due to the low energy of the coherent interface between the epitaxial film and the substrate. The critical thickness of the stabilised phase decreases with an increase in the energy difference between the stable and unstable phases: even in thin films of the $GdMnO_3$ hexagonal phase, the upper layer has a perovskite structure. In the $EuMnO_3$ films, the layer of the stabilised hexagonal phase is even thinner.

We have also prepared previously unknown orthoferrites with the hexagonal structure, $RFeO_3$ (R = Eu, Er, Tm, Yb, Lu),[69] by stabilising them on the (111)$ZrO_2(Y_2O_3)$ substrate and confirmed, as in the case of manganites, the key conclusions of the thermodynamic model of ES. It was shown that these compounds may, in principle, exhibit ferroelecteric properties.[69]

The nickelates $RNiO_3$. A general structure–thermodynamics relationship for series of perovskite compounds has now been established, in particular, deformation of the perovskite structure with a decrease in the tolerance factor is accompanied by a decrease in the thermodynamic stability of compounds.[70] In the series of lanthanide perovskites (nickelates and cobaltites), this is manifested as an increase in the equilibrium pressure of oxygen

(for T = const) following a decrease in the lanthanide ionic radius. The solid-state synthesis of $RNiO_3$ powder or ceramics, except for $LaNiO_3$, requires high pressure P_{O_2}, which reaches 100 bar for the last members of the lanthanide row.

Using the ES, we succeeded in preparing thin epitaxial films of $RNiO_3$ (R = Pr, Nd, Sm, Gd) at a reduced oxygen pressure, which did not exceed 20 mbar.[71] The formation of perovskite phases was observed only for substrates having a perovskite structure ($LaAlO_3$, $SrTiO_3$), whereas the films grown on MgO and $ZrO_2(Y_2O_3)$ consisted of a mixture of the R_2O_3 and NiO oxides. Single-phase $RNiO_3$ films were prepared only on the $LaAlO_3$ substrate, which is most consistent with nickelates as regards the crystal lattice parameter ($\varepsilon = 0.2\% - 0.7\%$), whereas on the $SrTiO_3$ substrate with greater ε ($\varepsilon \approx 3\%$), phases of simple nickel and lanthanide oxides are formed in addition to $RNiO_3$ perovskite (Fig. 9). The content of the epitaxial perovskite $RNiO_3$ phase in the films prepared by MOCVD under identical conditions decreased with a decrease in the ionic radius of R^{3+}, due to the decrease in the perovskite stability in the same series.[72, 73] The least stable nickelate we studied, $GdNiO_3$, could be obtained only on $LaAlO_3$. These experiments revealed a clear-cut correlation between the thermodynamic properties of nickelates (the measure of their instability) and the critical film thickness for stabilised phases, which is consistent with the ES theory considered above.[67] After the critical thickness had been attained, a layer of the R_2O_3 and NiO oxide mixture started to grow on the surface of the perovskite phase.

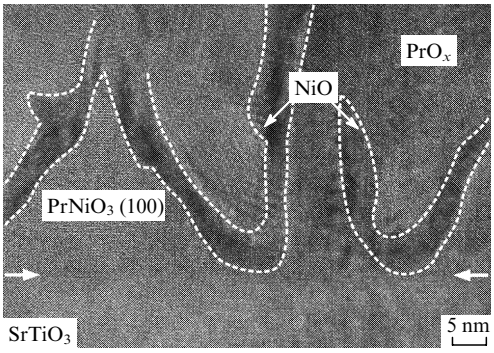


Figure 9. Cross-section of the $PrNiO_3/(100)SrTiO_3$ film in the (100) plane obtained by HREM (see the comments in the text).

Important information was gained from a HREM study of cross-sections of nickelate films. It was found that the atomically smooth interface between the epitaxial $RNiO_3$ film and the $LaAlO_3$ substrate is not distorted by misfit dislocations, which indicates unambiguously the presence of epitaxial compression stresses in the films, resulting in the tetragonal deformation of the film crystal lattice. Previously, this type of deformation has been found by X-ray diffraction.[74] It was demonstrated that nickelates crystallise in an orthorombic group of symmetry *Pnma*. It was shown that epitaxial films of nickelates (like manganite films) consist of orthorhombic domains; the axis directed along the doubled cell parameter can be oriented along the three orthogonal axes (Fig. 10) ¶ and the ε parameters for all the possible domain orientations are virtually equal. In this case, the formation of orthorhombic domains (twins) in nickelate films does not eliminate the epitaxial stresses (the situation opposite to that described above for $RMnO_3$ perovskite films). As a result, the anisotropic epitaxial stresses represent one more factor (in addition to the misfit of the lattice parameters at the film/substrate interface) to restrict the critical thickness of the stabilised phase.

¶ Note that orthorhombic distortions in lanthanide nickelates are much less pronounced than in manganites.

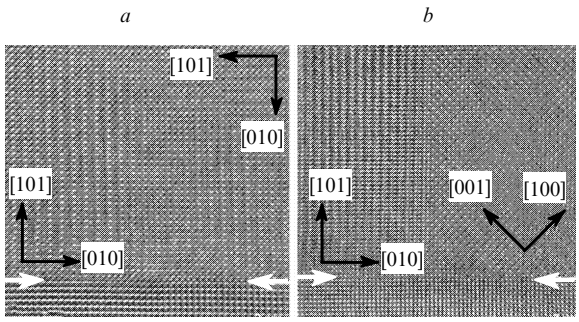


Figure 10. Domain structure of the $SmNiO_3/(001)LaAlO_3$ film (according to HREM data).
(*a*, *b*) Different domain orientations are shown.

An HREM study of the cross-sections of the films has also shown that the perovskite phase coexists, in some range of thicknesses, with simple oxide phases (see Fig. 9) and the volume fraction of perovskite gradually decreases with an increase in the film thickness. This result attests to the limitation of the model in which the phase composition sharply changes as the film reaches the critical thickness h_c and, conversely, validates the idea put forward by Little and Zangwill,[49] which predicts gradual transition from the epitaxially stabilised phase to phases stable as bulk materials.

The cobaltates $RCoO_3$. In the series of $RCoO_3$ perovskites, the border of high-temperature stability of phases at $P_{O_2} = 1$ bar is situated between Yb and Tm; hence, the last members of the row, $YbCoO_3$ and $LuCoO_3$, can be obtained by solid-state synthesis only under an elevated pressure of oxygen.[75] An estimate of the Gibbs energy for the reactions

$$Co_3O_4 + R_2O_3 + O_2 \longrightarrow RCoO_3$$

R = Tm – Lu

by extrapolation of the linear dependence of $\Delta G^\circ_{1100\,K}$ on the tolerance factor[76] obtained for more stable cobaltates gives positive values. In particular, the $\Delta G^\circ_{1100\,K}$ value for the least stable $LuCoO_3$ is equal to 8 kJ mol^{-1}, which confirms that this compound is unstable under solid-state synthesis conditions.

We attempted to prepare $LuCoO_3$ films by epitaxial stabilisation without using a high pressure of oxygen. The films were synthesised by MOCVD at 700 – 850 °C and P_{O_2} = 6.5 mbar on single-crystalline substrates, $(001)CaGdAlO_4$, $(001)LaAlO_3$, $(001)SrTiO_3$ and (001)MgO,[77] whose parameters ε were 0.3%, 3%, 6% and 14%, respectively. The X-ray diffraction patterns of $LuCoO_3$ films (Fig. 11), obtained on different substrates at the same temperature, imply a dependence of the formation of $LuCoO_3$ on the ε value. Indeed, a film of the Lu_2O_3 and Co_3O_4 oxide mixture grew on the non-coherent MgO substrate, while the films grown on more coherent $SrTiO_3$, $LaAlO_3$ and $CaGdAlO_4$ substrates were epitaxial $LuCoO_3$ films with the perovskite structure in the (001) orientation with an admixture of simple oxides, the content of the admixture decreasing on passing from $SrTiO_3$ to $CaGdAlO_4$ (one should note a low intensity of reflections from polycrystalline phases in the films). Similar results were obtained in the synthesis of $TmCoO_3$ films. However, the films of more stable $GdCoO_3$ with $\Delta G^\circ_{1100\,K} < 0$ [76] were also grown on MgO, moreover, in the polycrystalline form, *i.e.*, without the directing effect of the substrate.

An increase in the temperature of film deposition resulted in disappearance of the perovskite phase due to an increase in the equilibrium oxygen pressure above cobaltates. However, in this case, too, the behaviours of the films grown on different substrates were markedly dissimilar: the film stabilisation energy was correlated with ε. On the $CaGdAlO_4$ substrate, the perovskite phase was observed even at 820 °C, whereas on $SrTiO_3$, this phase did

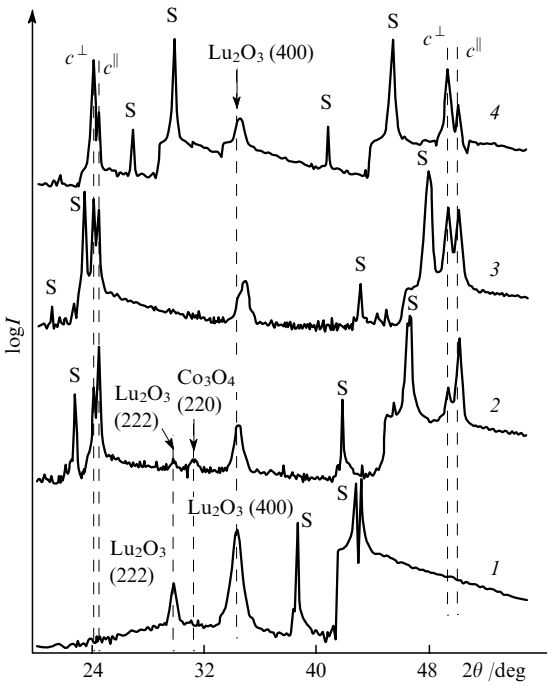


Figure 11. X-Ray diffraction patterns of the $LuCoO_3$ films grown on various substrates (S is the substrate reflections, $c^{\parallel}$, $c^{\perp}$ are perovskite reflections).
Substrate [ε (%)]: (*1*) (001)MgO (14), (*2*) (001)$SrTiO_3$ (6), (*3*) (001)$LaAlO_3$ (pseudo-cubic notation) (3), (*4*) $CaGdAlO_4$ (0.3).

not exist above 800 °C. The process of disappearance of the stabilised $LuCoO_3$ film on raising the deposition temperature differed from the process of disappearance of the bulk dissociating oxide: the latter disappeared immediately after some threshold $P_{O_2}-T$ conditions (equilibrium dissociation conditions). In the case of films, the intensity of X-ray reflections from $LuCoO_3$ gradually decreases with temperature rise; this is in line with the decrease in the critical thickness of the stabilised phase following a decrease in the thermodynamic stability of this phase [*i.e.*, with an increase in $\Delta g''_V - \Delta g'_V$, see Eqn (9)].

Evidently, even at the optimal temperature of film deposition (750 °C) on the most coherent substrate, an admixture-free $LuCoO_3$ perovskite phase can be obtained only in a limited range of thicknesses. When the film thickness is ~100 nm, the films contain only the perovskite phase, whereas ~400-nm thick films contain pronounced amounts of Lu_2O_3 and Co_3O_4 impurities. These are equilibrium phases (under film deposition conditions) of the bulk polycrystalline Lu–Co–O system formed in the upper layers of the $LuCoO_3$ films as they exceed the critical thickness.

The essential orthorhombicity inherent in the $RCoO_3$ phases is responsible for the doubling of the diffraction peak for the cubic perovskite. The orientation of the orthorhombic domains in epitaxially stabilised films depends on the nature of the substrate. According to X-ray diffraction data, two types of domains are formed in the $LuCoO_3$ films: in the first-type domains ($c^{\parallel}$), the doubled parameter (*i.e.*, the *c* axis within the *Pbnm* group) is directed along the substrate surface, while in second-type domains ($c^{\perp}$), it is perpendicular to the substrate. It was found that the fraction of $c^{\parallel}$-type domains increases in the series $CaGdAlO_4$–$LaAlO_3$–$SrTiO_3$, whereas the fraction of $c^{\perp}$-type domains decreases in this series (see Fig. 11). This regularity was interpreted by mininisation of the misfit between the film and substrate parameters through giving preference to either type of domains. This raised the question of whether both types of domains originate simultaneously during film deposition, or twinning occurs during cooling of the films. The X-ray diffraction analysis of the films quenched after deposition at 800 °C has shown that single-domain films of the $c^{\parallel}$ type originate and grow on $SrTiO_3$, and $c^{\perp}$ type films grow on $LaAlO_3$ (Fig. 12). The structure of twin domains is formed during cooling, apparently according to the martensite mechanism. Twinning is a way of decreasing thermomechanical stresses arising at the film/substrate interface on slow cooling.[77]

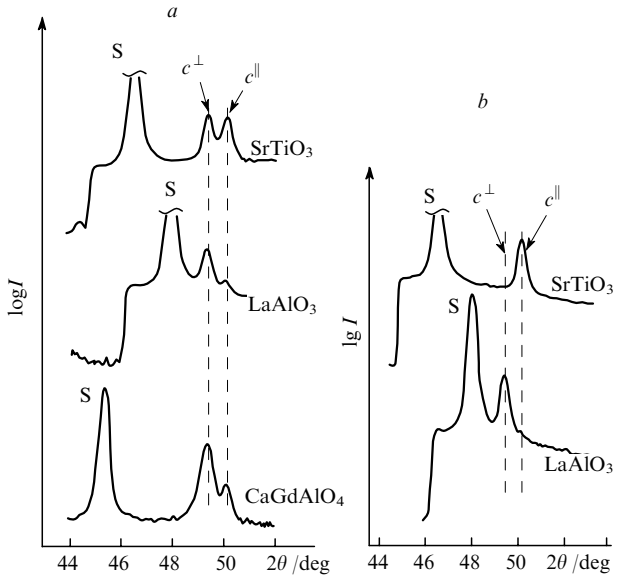


Figure 12. Sections of the X-ray diffraction patterns of the $LuCoO_3$ films on various substrates.
(*a*) X-ray diffraction patterns of the films slowly cooled after deposition; (*b*) X-ray diffraction patterns of the films hardened after deposition on the substrate at 800 °C in air. The reflection (220) refers to type $c^{\perp}$ domain and (004), to type $c^{\parallel}$ domain.

The indates $RInO_3$. The lanthanide indates of the composition $RInO_3$, existing in the bulk state, can be divided into three groups in terms of the structure, namely, perovskites, hexagonal phases and fluorite type phases. The compounds $RInO_3$ with R = La–Sm can be prepared as perovskites by the conventional solid-state synthesis, whereas the homologues with R = Eu–Dy form hexagonal phases under the same conditions. Under the action of high pressure (65 kbar), these phases can turn into perovskites.[78] The compounds $RInO_3$ with R = Y and Ho are solid solutions of the fluorite type, which also acquire a perovskite structure under the action of high pressure.[79] No data on the phase formation in the R–In–O systems (R = Er–Lu) have been reported.

We attempted to synthesise indates $RInO_3$ (R = Eu–Lu) with the perovskite structure without using high pressure but by means of the ES.

As the substrate for growing $RInO_3$ films, we chose $SrTiO_3$, which best fits the known perovskites $RInO_3$ as regards the cell parameter. We have grown $RInO_3$ films (R = Eu–Lu) on this substrate. Figure 13 shows X-ray diffraction spectra of the resulting films, which confirm their perovskite structure [reflections (001) and (002)], and the photomicrograph of the $NdInO_3/SrTiO_3$ film, which proves that the h_c value is greater than 80 nm. The decrease in the intensity of perovskite reflections (002) upon a decrease in the ionic radius of R^{3+} indicates that the stability of perovskites decreases with an increase in the tolerance factor and that the critical thickness of the stabilised perovskite phases decreases as they become less stable in the form of bulk materials. It was found that the conductivity of the resulting thin films of lanthanide indates can be appreciably changed by heterovalent doping. The doped films can be used in gas sensors.

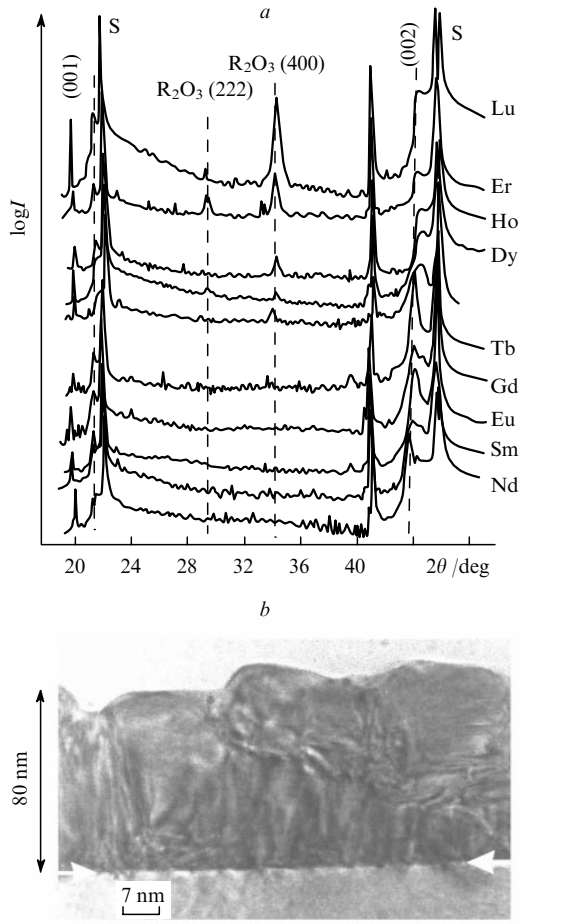


Figure 13. X-Ray diffraction patterns of the $RInO_3$ films (R = Nd – Lu) grown on $SrTiO_3$ (*a*) and photomicrograph of the $NdInO_3/SrTiO_3$ film (*b*) obtained by HREM.

The garnets $R_3Fe_5O_{12}$. A necessary condition for the formation of a garnet structure is fulfillment of the criterion $r_{M^{3+}} : r_{Fe^{3+}} \leqslant 1.7$, which means that ferrogarnets are formed only in those cases where the ionic radius of the lanthanide is not larger than 1.14 Å, *i.e.*, only for R = Sm – Lu, Y. The elements of the beginning of the row (La, Ce, Pr, Nd) do not form garnets in the conventional solid-state synthesis, although $Nd_3Fe_5O_{12}$ can be synthesised at high pressure.[80]

We managed to prepare (by means of the ES) thin films of garnet-type solid solutions $(La_xNd_{1-x})_3Fe_5O_{12}$ on the $(111)Gd_3Ga_5O_{12}$, $(210)Gd_3Ga_5O_{12}$, $(111)Nd_3Ga_5O_{12}$ and $(111)(Y_{0.8}Ca_{0.9}Tm_{0.7}Sm_{0.6})(Ge_{0.2}Fe_{0.8})_5O_{12}$ substrates with a garnet structure; the orientation of the garnet films corresponded to the substrate orientation (no garnet phase was formed in films with the same composition on substrates with the perovskite or MgO structure).

The photomicrographs of the $(La_xNd_{1-x})_3Fe_5O_{12}$ films (Fig. 14) give an idea of the critical film thickness of stabilised garnets. In the case of $Nd_3Fe_5O_{12}$, the film thickness was unexpectedly great (more than 3.6 μm, Fig. 14 *b*). It was found that the film thickness decreases with an increase in the La concentration in the solid solution (Fig. 14 *c*). When the critical thickness is exceeded, $RFeO_3$ and Fe_2O_3 equilibrium phases start to grow on the surface of the stabilised phase of the garnet.

The concentration ranges of stability of the garnets $(La_xNd_{1-x})_3Fe_5O_{12}$ grown on substrates with the garnet structure were determined using powder X-ray diffraction and HREM (Fig. 14). It was found that films with the garnet structure are formed only in the range of $0 < x < 0.66$. Differences in the

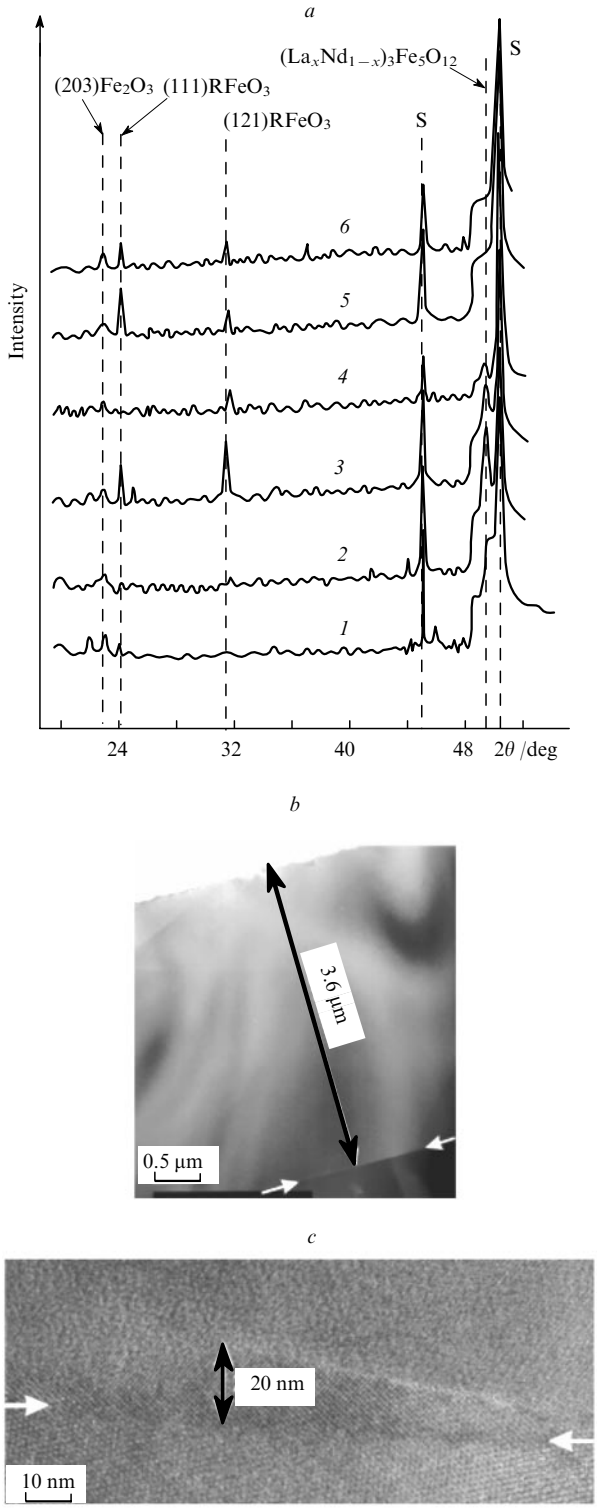


Figure 14. Formation of garnet phases $(La_xNd_{1-x})_3Fe_5O_{12}$.
(*a*) X-ray diffraction patterns of films on the $(111)Gd_3Ga_5O_{12}$ substrate, $x = 0$ (*1*), 0.37 (*2*), 0.5 (*3*), 0.66 (*4*), 0.7 (*5*), 0.75 (*6*);
(*b*, *c*) photomicrographs (TEM) of the cross-sections of films recorded along the ⟨110⟩ direction; $x = 0$ (*b*) and 0.66 (*c*).

substrate material do not much influence the stability limits of the $(La_xNd_{1-x})_3Fe_5O_{12}$ phases.

Epitaxially stabilised lanthanide-derived ferrogarnets, which are soft ferromagnetic materials, can find application in devices for amplification of an external magnetic field and in thin-film magnetooptical devices.

5. Application of epitaxial stabilisation for the development of functional heterostructures (selective epitaxy)

Epitaxial stabilisation can be used successfully for the design of multilayer heterostructures in selective epitaxy processes. The selective epitaxy is performed on specially prepared areas of the substrate which are characterised by structural coherence with the stabilised phase. On those substrate sections where the coherence condition is not fulfilled, products would crystallise that correspond to the equilibrium bulk state of the system. An example of such application of the ES is reported in our study [81] aimed at designing a heterostructure composed of numerous alternating lanthanide manganite and nickelate ribbons. This heterostructure shows an unusual temperature dependence of the resistivity (Fig. 15, curve *1*), because it combines the manganite phase (curve *2*), characterised by a sharp decrease in the resistivity on the dielectric–metal transition, and the nickelate phase (curve *3*), whose resistivity, conversely, sharply increases below the temperature of the metal–dielectric transition. As a result, the temperature behaviour of the resistivity of this heterostructure exhibits a sharp minimum.

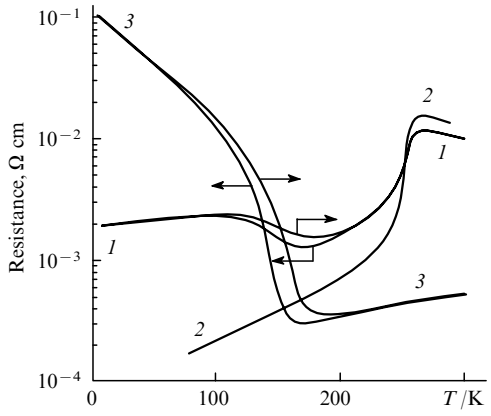


Figure 15. Temperature dependence of the resistance of the $NdNiO_3$–$La_{0.7}Ca_{0.3}MnO_3$ heterostructure (*1*) and its components $La_{0.7}Ca_{0.3}MnO_3$ (*2*) and $NdNiO_3$ (*3*).

The heterostructure was formed using MOCVD and photolithography (Fig. 16). First, the epitaxial $(La,Pr)_{0.7}Ca_{0.3}MnO_3$ layer was formed on the $LaAlO_3$ substrate (Fig. 16 *a*). Then this layer was etched with H_2O_2 and H_2SO_4 solutions through a photolitographic mask (Fig. 16 *b*), a polycrystalline layer of CuO was applied on it (Fig. 16 *c*), and the spots meant for $NdNiO_3$ were etched with an HCl solution (Fig. 16 *d*). The etching resulted in exposure of areas on the surfaces of the perovskite substrate and the manganite layer; hence, during the subsequent deposition of $NdNiO_3$, perovskite phase grew epitaxially exactly on these areas (Fig. 16 *e*), while an equilibrium mixture of the Nd_2CuO_4 and NiO phases with high resistivity was situated on the surface bearing the remaining CuO (structurally non-coherent to perovskite). The current that was passed along the substrate surface ran succesively through the alternating manganite and nickelate regions.

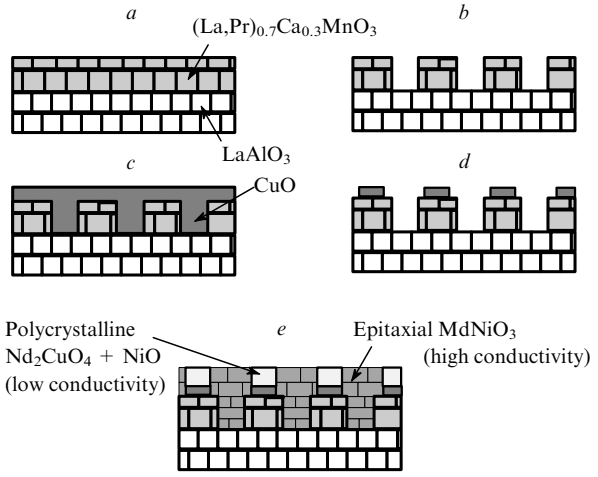


Figure 16. Formation of the manganite/nickelate heterostructure [for the description of stages (*a*–*e*), see the text].

It should be noted that in the epitaxial stabilisation of these heterostructures, one should take into account the stressed state of the substrate ($LaAlO_3$) surface and the buffer layer [$(La,Pr)_{0.7}Ca_{0.3}MnO_3$]: with the same deposition conditions and the same composition of the deposited components, different types of these stresses may completely change the phase composition of the deposited layer. Thus the epitaxial $NdNiO_3$ films obtained on a buffer manganite layer, $(La,Pr)_{0.7}Ca_{0.3}MnO_3$, which was, in turn, deposited on the perovskite $LaAlO_3$ and $SrTiO_3$ substrates were substantially dissimilar. Quite perfect epitaxial layers of $NdNiO_3$ up to a thickness of 200 nm were obtained on the $(La,Pr)_{0.7}Ca_{0.3}MnO_3/LaAlO_3$ substrates, whereas in the case of $(La,Pr)_{0.7}Ca_{0.3}MnO_3/SrTiO_3$, the perovskite phase contained simple oxides even at early stages of the growth (films with a similar phase composition were grown on the $SrTiO_3$ substrate without a buffer layer [82]). The epitaxial quality of the $(La,Pr)_{0.7}Ca_{0.3}MnO_3$ buffer layer grown on both substrates was equally high; however, the epitaxial stresses in the layers had opposite signs on different substrates, namely the buffer layer on $LaAlO_3$ experienced compression and that on $SrTiO_3$ underwent stretching in the substrate plane. This is indicated unambiguously by comparison of the lattice parameters of the non-deformed $(La,Pr)_{0.7}Ca_{0.3}MnO_3$ layer ($a = 0.385$ nm) with those of the $(La,Pr)_{0.7}Ca_{0.3}MnO_3/LaAlO_3$ ($a = 0.383$ nm) and $(La,Pr)_{0.7}Ca_{0.3}MnO_3/SrTiO_3$ ($a = 0.387$ nm) layers. The lattice parameter of the compressed $(La,Pr)_{0.7}Ca_{0.3}MnO_3/LaAlO_3$ layer is much closer to that of $NdNiO_3$ ($a = 0.381$ nm) than the parameter of the stretched layer, which accounts for the better properties of the former in stabilisation of the nickelate perovskite phase.

6. Effect of the epitaxy on the mutual solubility of oxides

The change in the phase equilibria in oxide systems under the influence of epitaxy is encountered rather often. However, we have not yet mentioned the possibility of extending the homogeneity regions for the cations of the epitaxially stabilised phases.† Below we consider several typical examples.

$R_{1-x}MnO_{3+\delta}$ (R = La, Nd). The perovskite $R_{1-x}MnO_{3+\delta}$ phases formed by lanthanides with a great ionic radius can be markedly non-stoichiometric as regards the cations,[83] the excess negative charge being counterbalanced by the transition $Mn^{3+} \rightarrow Mn^{4+}$. The maximum allowable lanthanide deficiency in the $R_{1-x}MnO_{3+\delta}$ ceramic samples corresponds to the subscript $x = 0.1-0.15$ (the x value depends on the conditions of high-temperature treatment; the highest non-stoichiometry can be attained under oxidative conditions). The epitaxial $R_{1-x}MnO_{3+\delta}$ films prepared by MOCVD on the $LaAlO_3$ and $SrTiO_3$ substrates allow a much higher deficiency of lanthanide ions. For example, single-phase perovskite $R_{1-x}MnO_{3+\delta}$ films (R = La, Nd) with $x \leqslant 0.3$ have been synthesised.[84]

$Zn_{1-x}M_xO$ (M = Mg, Mn). In wurtzite (ZnO), zinc can be partially replaced by other cations with similar ion radii such as Mg^{2+}, Cd^{2+} or Mn^{2+}. In ceramic $Zn_{1-x}Mg_xO$ samples, the x value does not exceed 0.02–0.04,[85] while in single-phase (0001)$Zn_{1-x}Mg_xO$ epitaxial films obtained by MBE at

† In this case, the term 'stabilised phases' is used to mean not only phases that cannot be obtained in the bulk state under the given thermodynamic conditions but also stable phases whose thermodynamic properties have changed in the epitaxially bound state.

550 °C,[86–88] the x values reach 0.22 and for the films obtained by PLD at 700–750 °C,[88] $x \leqslant 0.36$. The difference in the mutual solubility of the ZnO and MgO oxides in ceramics and epitaxial films is emphasised by the fact that two-phase ceramic pellets were used as targets (the sources of ZnO and MgO vapours). The epitaxial films were grown on the $(0001)Al_2O_3$ substrate. The film thickness reached 150 nm[86–88] and $\leqslant$500 nm.[89] The epitaxial relations for the ZnO–MgO solid solution reported in the literature[89]

$$(0001)[\bar{1}2\bar{1}0]Zn_{1-x}Mg_xO \parallel (0001)[01\bar{1}0]Al_2O_3$$

coincide with those for the films of pure ZnO grown on sapphire.[90] This mutual orientation of the film and the substrate corresponds to a misfit of the parameters $\varepsilon = 15\%$ which induces a substantial dislocation density at the interface.[89] In addition, it was shown that the $Zn_{0.85}Mg_{0.15}O$ film is stable during annealing (1000 °C, $P_{O_2} = 1$ bar, 1 h), whereas the film with the composition $Zn_{0.78}Mg_{0.22}O$ decomposes under the same conditions to give an equilibrium mixture of the wurtzite solid solution $Zn_{0.85}Mg_{0.15}O$ and the solid solution $Mg_{0.46}Zn_{0.54}O$ with the NaCl structure.[88] Thus, the extension of the wurtzite solid solution in the ZnO–MgO system markedly increases as a result of the ES.

The synthesis of epitaxial films of wurtzite doped with manganese oxide, $(0001)Zn_{1-x}Mn_xO/(0001)Al_2O_3$, has been reported.[91] Films several hundred nanometres thick were obtained at 600 °C. It was found that the unit cell parameters of wurtzite (a and c) increased monotonically with an increase in the Mn content up to $x = 0.35$; this markedly exceeds the solubility level of manganese oxide in zinc oxide in equilibrium bulk systems, which corresponds to $x_{lim} = 0.13$.[92]

$Ni_xFe_{3-x}O_4$. Nickel oxide NiO, like iron oxide Fe_3O_4 (spinel type), can grow epitaxially on the MgO substrate; however, the parameters of Fe_3O_4 are in better agreement with the substrate parameters; therefore, the spinel type solid solution $Ni_xFe_{3-x}O_4$ is stabilised on the substrate. The limiting nickel content in the solution is higher than in equilibrium polycrystalline solid solutions under the same conditions. The distribution of the Ni and Fe atoms over tetrahedral and octahedral positions of the spinel structure differs appreciably from that in the bulk materials.[93] This indicates that the ES can substantially influence the degree of inversion of spinels and, correspondingly, their magnetic properties.

$BaRuO_3$–$SrRuO_3$. From consideration of the equilibrium phase diagram of the $BaRuO_3$–$SrRuO_3$ binary system, one can predict the formation of two immiscible solid solutions, namely, the perovskite solution based on $SrRuO_3$ and stable up to Ba : Sr = 1 : 1 and a hexagonal (polytype 9R) solution based on $BaRuO_3$ and stable up to Ba : Sr = 9 : 1.[94] The preparation of a continuous series of solid solutions of the perovskite type, from $SrRuO_3$ to $BaRuO_3$, by radio frequency sputtering on the $SrTiO_3$ substrate has been reported.[17] However, an attempt to prepare $BaRuO_3$ as a perovskite on the $(001)KTaO_3$ perovskite substrate ($a = 0.3989$ nm) failed. This may be due to the fact that $BaRuO_3$ in the perovskite form experiences pronounced tetragonal distortions; as a result, its lattice becomes more consistent with the $SrTiO_3$ lattice than with the $KTaO_3$ lattice.

These examples provide the conclusion that solid solutions in epitaxial films are more extended than the same solid solutions in powders, ceramics, single crystals or polycrystalline films. The degree to which the ES extends the homogeneity regions depends on the coherence of the structures of the resulting film and the substrate and on the enthalpy of formation of the solid solution. If the consideration is restricted to the formation of regular solid solutions for which $\Delta H = x_A x_B Q$ (where x_A and x_B are the mole fractions of the components, Q is the energy parameter of interaction independent of the composition), it can be stated that the smaller the Q value (which is always positive), the more pronounced the effect of epitaxial extension of the solubility limits. In some cases, continuous solid solutions can be prepared.

7. The effect of epitaxy on the reactivity of thin films

The set of experimental data considered in this review attests that the $P–T–x$ space of thermodynamically stable existence is greater for the epitaxial phase than for its substrate-free bulk state. This implies that the chemical potential of the epitaxially bound phase (μ_{el}) is lower than the standard chemical potential (μ^0) of the same phase. In view of the fact that

$$\mu_{el} = \mu^0 + RT\ln a_{el},$$

the thermodynamic activity of the phase in the epitaxial state is given by $a_{el} < 1$. Thus, the epitaxial binding of some phase by a coherent substrate has the same consequence (namely, a decrease in the thermodynamic activity of the phase) as the formation of a solid solution or a chemical compound by this phase. A decrease in the thermodynamic activity of the phase in the epitaxial state ($a_{el} < 1$) implies a decrease in its reactivity compared to that of the substrate-free phase. It should be emphasised that this conclusion is valid not only for the 'unusual phases' which can arise under these conditions only owing to the ES but also for any epitaxial phases, no matter whether they are stable in the free (bulk) state.

The chemical consequences of the reduced thermodynamic activity may vary. In particular, the dissociation equilibrium

$$ABO_x \rightleftharpoons AO + BO_{x-1} + O_2$$

would be shifted more appreciably to the left in the case of epitaxial films than for the same phases in the bulk state at the same $P_{O_2}–T$ conditions (in other words, at the same temperature, the equilibrium pressure of oxygen P_{O_2} above an epitaxial film is lower than that above a powder or ceramic with the same composition).

In those cases where the growing phase is not stoichiometric for oxygen and dissociation does not result in the phase decomposition

$$ABO_x \rightleftharpoons ABO_{x-\delta} + \delta/2\,O_2,$$

one can expect that the epitaxial and bulk phases brought to equilibrium under the same $P_{O_2}–T$ conditions would differ in the oxygen content.‡

This conclusion may appear defamatory for the common practice of investigation of the dependence of the functional properties of films on the oxygen non-stoichiometry. Since the direct determination of the oxygen content in thin films is an exceptionally complicated analytical problem yet unsolved, the amount of oxygen is usually determined in the corresponding powders or ceramics, which can be easily analysed by both chemical and physical methods (the oxygen content in epitaxial films is considered to be the same as in powders and in ceramics after identical heat treatment). The observed differences between the functional properties (first of all, electric and magnetic ones) of epitaxial films and ceramics with the composition as close as possible to that of the films are interpreted most often as being due to different microstructures and/or stressed states of the films; however, the role of differences in the oxygen non-stoichiometry also cannot be neglected.

The problem becomes even more complicated if one takes into account the dependence of the thermodynamic properties of the epitaxial layer on its thickness; obviously, the difference $\mu^0 - \mu_{el}$ in each section parallel to the substrate plane should decrease on moving away from the film/substrate interface toward the upper surface of the film. For a non-stoichiometric oxide, this means, in particular, that the content of oxygen in an epitaxial film would vary along the thickness coordinate. Unfortunately, due to the lack of experimental data, this aspect can be discussed only as a problem definition.

‡ The quantitative difference between the oxygen contents is difficult to predict, because the uncertainties in the estimation of the energy benefit from the epitaxial growth in particular systems are rather high.

Below we elucidate how the decrease in the phase reactivity in the epitaxial state would influence the solid-state reactions involving them. We demonstrated that in the epitaxial heterostructures $YBa_2Cu_3O_{7-\delta}/CeO_2/R\text{-}Al_2O_3$, no chemical interaction takes place between the $YBa_2Cu_3O_{7-\delta}$ superconductor and the $(001)CeO_2$ buffer layer grown epitaxially on the *R*-sapphire, not even during the long-term high-temperature annealing (Fig. 17 *a*).[95,96] In addition, it is well known [97] that polycrystalline CeO_2 reacts with $YBa_2Cu_3O_{7-\delta}$ according to the reaction

$$3\,CeO_2 + 2\,YBa_2Cu_3O_{7-\delta} \longrightarrow 3\,BaCeO_3 + Y_2BaCuO_5 + 5\,CuO.$$

The Gibbs energy of this reaction calculated for conditions similar to the conditions of MOCVD [98] under which the epitaxial heterostructures were obtained ($T = 820$ °C and $P_{O_2} = 2$ mbar) equals -5 kJ mol^{-1}. This reaction will not take place if ΔG becomes positive. This will happen when $a_{CeO_2} \approx 0.83$. Apparently, such decrease in the activity of CeO_2 occurs during its epitaxial growth on *R*-sapphire.

If polycrystalline CeO_2 is replaced by ZrO_2, the following reaction will proceed at the $YBa_2Cu_3O_{7-\delta}/ZrO_2$ interface

$$3\,ZrO_2 + 2\,YBa_2Cu_3O_{7-\delta} \longrightarrow 3\,BaZrO_3 + Y_2BaCuO_5 + 5\,CuO.$$

The replacement of polycrystalline ZrO_2 by the epitaxial one does not terminate the reaction. The reason can be understood from thermodynamic considerations: the Gibbs energy ΔG for this reaction calculated for the MOCVD conditions [98] is equal to -30 kJ mol^{-1}. This energy remains negative even if $a_{ZrO_2} = 0.83$, *i.e.*, the reaction does not stop. It is of interest that the product of reaction of ZrO_2 with $YBa_2Cu_3O_{7-\delta}$, namely, compound $BaZrO_3$, which separates the superconductor layer from the ZrO_2 substrate, belongs to the perovskite type and, therefore, it forms epitaxial interfaces with both the $YBa_2Cu_3O_{7-\delta}$ film and the substrate (Fig. 17 *b*).

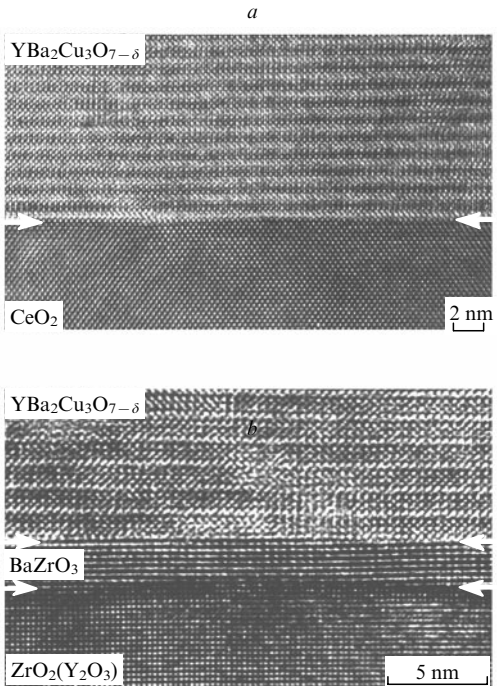


Figure 17. Images of the cross-sections of the $YBa_2Cu_3O_{7-\delta}$ films on CeO_2 (*a*) and on $ZrO_2(Y_2O_3)$ (*b*) (the images were obtained by HREM). (*a*) no chemical reaction takes place at the interface between the $YBa_2Cu_3O_{7-\delta}$ superconductor and the CeO_2 buffer layer, (*b*) a $BaZrO_3$ layer is formed at the interface.

III. Variant structures

During the last 15–20 years, vast experimental material has been accumulated on the heteroepitaxy of simple and complex oxides of various structures. The diversity of the crystal structures formed in the heteroepitaxy of oxides gives rise to a series of interesting phenomena not involved in classical metallic and semiconductor systems. For example, a definite type of orientational relations between an epitaxial film and a single-crystalline substrate can often be realised in different ways.

The orientational relations in heteroepitaxial systems are usually analysed in terms of the concept of coincident site lattices (CSL). Within the framework of this concept, the two-dimensional crystal lattices (site networks) of the film and the substrate are compared in the region of their contact.[99–101] Usually, an idealised view of the surface structure is invoked, *i.e.*, the structure of the surface of each crystal is regarded as being identical to the structure of a similar crystallographic plane inside the crystal, the rearrangement effects that took place on the exposed surface being ignored.[102] This simplification proved to be quite satisfactory, because the energy of the epitaxial surface is much lower than the energy of the free surface of the crystal. Therefore, the surface rearrangement is hampered due to overlaying of the epitaxial film.

Despite the diversity of the CSL sizes and shapes, they can always be reduced to one of five types of two-dimensional lattices (Fig. 18) corresponding to four types of symmetry (in the same way as three-dimensional lattices can be reduced to one of the 14 Bravais lattices, which form six systems). In the simplest case, the type of two-dimensional CSL coincides with the type of the two-dimensional lattice of the film and substrate site networks in the contact region. For example, for the epitaxial growth of the $(001)CeO_2$ film (fluorite structure) on the $(001)SrTiO_3$ substrate (perovskite structure), the site network and the CSL are square lattices. For $(001)CeO_2$, [100] and [010] are the CSL vectors, while for $(001)SrTiO_3$, these are [110] and [1$\bar{1}$0], respectively, *i.e.*, the *a* parameter of the CSL is $\sqrt{2}$ times greater than the lattice parameter of $SrTiO_3$.[103] In the example considered, this epitaxial relation is the only one possible; no other epitaxial relations arise in this case.

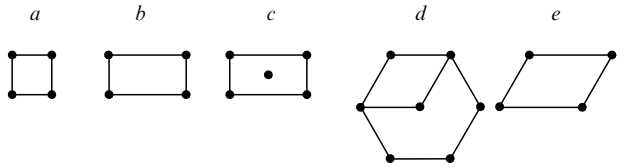


Figure 18. Types of two-dimensional lattices: primitive square (*a*), primitive orthogonal (*b*), centred orthogonal (*c*), primitive hexagonal (*d*), primitive oblique (*e*).

If the three-dimensional crystal lattices of the film and the substrate belong to different systems but the two-dimensional lattices correspond to the same system, in this case, too, only one epitaxial relation is realised. As an example, consider the $(001)TiO_2$ epitaxial films with a tetragonal anatase structure grown on perovskite substrates of the $(001)SrTiO_3$ type. This gives rise to the only possible square CSL with a spacing corresponding to that of the square site networks in the contact plane of the film and the substrate.[5,11,104]

Thus, a single variant of the CSL arises in those cases where the site networks of the film and the substrate in the contact plane correspond to the same system. If they are different, several variants of CSL fully equivalent from geometric and energetic standpoints may appear. The greatest possible number of variants is dictated by the order of the principal normal axis of the site

network that has a higher symmetry. It can be easily demonstrated that several equivalent CSL containing 2, 3, 4 and 6 epitaxial orientations can exist. The number of variants decreases if any additional symmetry elements in the film and substrate site networks coincide in the contact region (*e.g.*, symmetry planes parallel to the principal normal axis). The standard methods for determination of the number of variants of the epitaxial growth and orientation include X-ray diffraction (pole figures, φ-scanning), electron diffraction and transmission electron microscopy.

The formation of the variant structures is related genetically to the xenotaxy phenomenon (literally, this means a foreign growth on the surface), which represents the formation of a CSL, at the film/substrate interface, whose two-dimensional symmetry is lower than that allowed by the symmetry conditions. This situation is possible in the case where the low-symmetry configuration is clearly preferred from the energy standpoint. A low-symmetry CSL on a substrate site network with a higher symmetry also gives rise to variant structures. Depending on the relationship between the interface energies for the same film/substrate pair, different types of xenotaxy can arise, resulting in different variant structures.

Let us consider a simple example. During the deposition of films of the $RBa_2Cu_3O_{7-\delta}$ high-temperature superconductors (R is a lanthanide) on single-crystalline perovskite substrates in a pseudo-cubic (001) orientation (so-called *c*-orientation), the epitaxial growth of a film in the (100) orientation (*a*-orientation) is often observed. The smaller the misfit between the substrate and film lattice parameters (*i.e.*, the better the CSL coincidence), the easier the switching from the thermodynamically preferred growth along the (001) direction to the growth along the (100) direction (Fig. 19).[105–107] The site network of the perovskite substrate in the (001) plane is square. The $RBa_2Cu_3O_{7-\delta}$ site network in the (100) plane and the CSL are orthogonal and the ratio of their unit cell edges is close to 1 : 3. The maximum number of variants of the epitaxial growth for this case is 4, but the condition of collinearity of the perovskite and $RBa_2Cu_3O_{7-\delta}$ site networks reduces the possible number of variants to two:

$$(001)[100]SrTiO_3 \parallel (100)[001]RBa_2Cu_3O_{7-\delta}$$

and

$$(001)[010]SrTiO_3 \parallel (100)[001]RBa_2Cu_3O_{7-\delta}.$$

The existence of structural variants in the *a*-oriented $RBa_2Cu_3O_{7-\delta}$ films is responsible for the substantial difference between their electric properties and those of the *c*-oriented films with the same chemical composition. The critical current density in two-variant *a*-oriented $RBa_2Cu_3O_{7-\delta}$ films does not exceed 10^5 A cm^{-2} at 77 K, whereas in the monovariant *c*-oriented samples, this value reaches $\geqslant 10^6$ A cm^{-2} (see the studies [108, 109]). This difference is not at all due to the poor crystallinity of the two-variant structure compared to the monovariant one; conversely, the X-ray diffraction and HREM data indicate unambiguously that the *a*-oriented films are structurally more perfect (in particular, the integral width of the X-ray rocking curves is several times smaller for these films than for the *c*-oriented $RBa_2Cu_3O_{7-\delta}$ films). The decrease in the critical current density is due to the fact that in the HTSC structure, the superconducting carriers move efficiently only in the CuO_2 planes normal to the *c* axis. Thus, in the *c*-oriented films, the superconductive planes are stretched along the substrate plane. In the two-variant structure with the *a*-orientation, more intricate routes for the supercurrent are formed, *i.e.*, 'superconducting tapes', perpendicular to the substrate plane; this decreases the supercurrent critical density.

More complex variant structures are formed on the deposition of films of the perovskite series (for example, manganites $R_{1-x}A_xMnO_3$ (R is lanthanide, A is the alkaline earth element), cobaltites $R_{1-x}Sr_xCoO_3$ and ruthenates $CaRuO_3$ and $SrRuO_3$) [58] on substrates with the fluorite structure. The fluorite site network in the (001) plane is square. On the given surface these perovskites form an orthogonal site network in the (110) plane. The vectors of the orthogonal CSL are as follows: for the (001)$ZrO_2(Y_2O_3)$ fluorite, $[1\bar{1}0]$ and $4\times[\bar{1}\bar{1}0]$; for the (110) perovskites, $[1\bar{1}1]$ and $3\times[1\bar{1}\bar{2}]$ (Fig. 20). The similarity of the lengths of the body diagonal in the perovskite cube $[1\bar{1}\bar{2}]$ and the face diagonal in the fluorite cube $[1\bar{1}1]$ is the crucial factor for this type of epitaxial growth. However, a better dimensional fit may be observed in the perpendicular direction to the interface. For example, in the growth of (110)$La_{0.7}Ca_{0.3}MnO_3$ films on the surface of (001)$ZrO_2(Y_2O_3)$, the misfit in the CSL is 8% for the $[1\bar{1}0]$ and $[1\bar{1}1]$ pair and 2% for the $[\bar{1}\bar{1}0]$ and $[1\bar{1}\bar{2}]$ pair. The number of epitaxial variants for this case is 4 (Fig. 20). These variants are fully equivalent from the geometric and energetic standpoints. The HREM data (Fig. 21) indicate that these growth variants occur in the film as nanodomains (f1 and f2) with a characteristic size of 20–50 nm (Fig. 21 *c*). Interestingly, their lateral size almost does not change with thickness and the mutual coherence of the domains along the substrate surface normal is retained throughout the whole film thickness (Fig. 21 *d*).[110]

The formation of four-variant structures in the epitaxy of perovskites on the (001)fluorite has also been reported in a

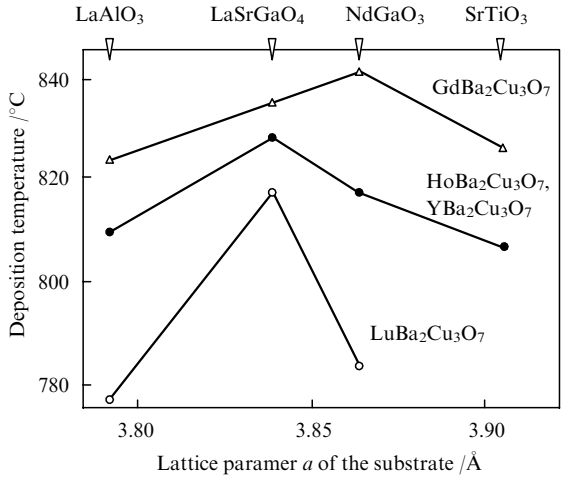


Figure 19. Temperature regions corresponding to the *c*-oriented epitaxial growth (above the line) and the growth with mixed *c* + *a*-orientation (below the line) of the $RBa_2Cu_3O_{7-\delta}$ films on substrates with a small (< 2%) misfit of parameters at the interface.

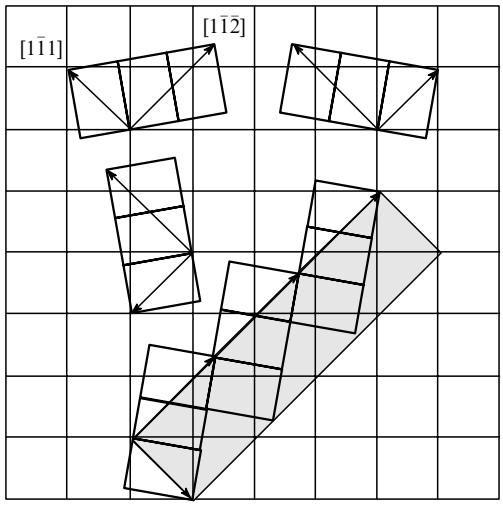


Figure 20. Four variants of perovskite growth on the (100)fluorite. The hatched region shows the CSL unit cell.

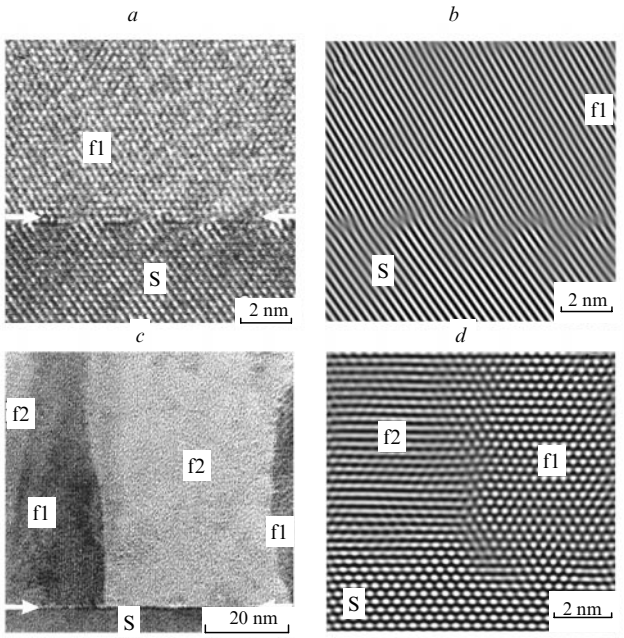


Figure 21. HREM study of the variant $(La_{0.5}Pr_{0.5})_{0.7}Ca_{0.3}MnO_3$ film on $(001)ZrO_2(Y_2O_3)$. In all cases, the $[110]ZrO_2(Y_2O_3)$ area is shown: (*a*) epitaxial stresses completely relax at the film/substrate interface, (*b*) Fourier image of the same region of the interface, (*c*) orientational growth modes (domains f1 and f2) in a low resolution, (*d*) coherence of the oriented variants along the film growth direction.

number of studies [111–114] dealing with the preparation of epitaxial films of the $Ba_{0.5}Sr_{0.5}TiO_3$, $Bi_{3.25}La_{0.75}Ti_3O_{12}$ and $SrBi_2TaO_9$ ferroelectrics with a ferroelectric polarisation axis oriented normal to the surface of the (001)silicon substrate. For solving this highly topical problem, epitaxial film heterostructures of the $(100)Bi_{3.25}La_{0.75}Ti_3O_{12}/(110)SrRuO_3/(001)ZrO_2(Y_2O_3)/(001)Si$ type were prepared. The conductive layer of the $SrRuO_3$ perovskite had a four-variant structure; as a result, $Bi_{3.25}La_{0.75}Ti_3O_{12}$ a layered phase derived from perovskite grown on $SrRuO_3$, had 8 options of arrangement in the plane parallel to the substrate.

A large number of boundaries between numerous structural variants may have an adverse effect on the ferroelectric properties; therefore, the possibility of affecting the pattern of the variant structure by changing the CSL on the surface of the $ZrO_2(Y_2O_3)$ single crystal through its slight $(1-5^\circ)$ deviation from the (001) plane has been studied.[114] This expedient proved to be most efficient when the deviation was performed along the [110] direction; the number of epitaxial variants in the $(110)SrRuO_3$ film decreased to two. Obviously, this approach could also find application in the studies of other heteroepitaxial systems.

A multivariant growth motif is also observed in the deposition of $La_{0.7}Ca_{0.3}MnO_3$ on $(111)ZrO_2(Y_2O_3)$. In this case, the body diagonal of the perovskite cube also corresponds to the face diagonal of the fluorite cube at the interface. In this case, the vectors of the orthogonal CSL determined from X-ray diffraction and HREM data are $[\bar{1}01]$, $3\times[1\bar{2}1]$ for $(111)ZrO_2(Y_2O_3)$ and $[1\bar{1}1]$, $4\times[1\bar{1}\bar{2}]$ for the (110)perovskite. The misfit of the CSL equals 8% for the $[\bar{1}01]$ and $[1\bar{1}1]$ pair and 0% for the $[1\bar{2}1]$ and $[1\bar{1}\bar{2}]$ pair. The theoretical number of equivalent epitaxial variants for this case is six, and all these are actually encountered in the film (Fig. 22).

A direct consequence of the formation of epitaxial variant structures is the presence in the film of a high density of special high-angle boundaries. The set of angle orientations of such boundaries is strictly fixed and their concentration does not change over the film thickness. This represents the basic difference between the variant structures and polycrystalline materials in which the angle orientations of the boundaries make a broad

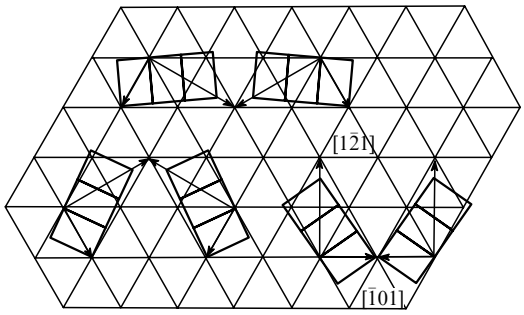


Figure 22. Six variants of the growth of perovskite on the (111)fluorite.

spectrum even in highly textured materials and the concentration of the boundaries themselves is not very high.

The epitaxial multivariant structure of the manganites is responsible for their interesting electrophysical properties which are not inherent in monovariant epitaxial films. First of all, this refers to the appearance of a substantial magnetoresistance (the change in the electric resistance of the material in a magnetic field) in weak magnetic fields over a broad temperature range below the Curie point.[115] This is due to the spin-dependent tunnelling of charge carriers through special high-angle boundaries. This is characteristic of the epitaxial films of manganites grown on bicrystalline perovskite substrates.[116]

The appearance of a substantial magnetoresistance in weak magnetic fields is of considerable interest as regards the manufacture of high-sensitivity magnetic field sensors. In the design of such sensors, one can use both the appearance of sharp maxima of positive magnetoresistance (*MR*) in the region of technical magnetisation (*i.e.*, magnetisation related to the re-orientation of magnetic domains) in fields weaker than 100 Œ and the appearance of great negative magnetoresistance ($\sim 30\%$) related to the tunnelling effect in fields of 100–5000 Œ (Fig. 23).

Both effects are also manifested in the traditional polycrystalline materials; however, the former requires much stronger fields (about 500–1000 Œ) and has a lower field gradient,[117] while the latter is much smaller in magnitude.[118] This is due to the fact that the structural coherence of high-angle boundaries implies a compression of the tunnelling barrier following an increase in the field strength,[119] which is impossible for non-coherent boundaries. We found that the magnitude of the tunnelling effect increases with an increase of the off-orientation angle of the neighbouring nanodomains in films with a variant structure.[109]

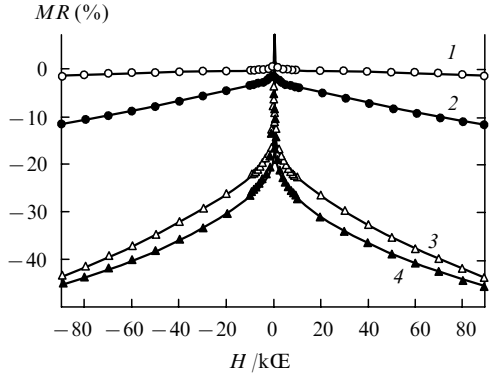


Figure 23. Magnetoresistance (*MR*) in the $(110)La_{0.7}Ca_{0.3}MnO_3$ epitaxial films grown on different substrates (temperature, 10 K). Substrate: (*1*) $(110)SrTiO_3$, (*2*) $(110)ZrO_2(Y_2O_3)$, (*3*) $(001)ZrO_2(Y_2O_3)$, (*4*) $(111)ZrO_2(Y_2O_3)$. Real structure of the obtained film: (*1*) monodomain, (*2–4*) multidomain with small-angle (*2*) and high-angle (*3*, *4*) boundaries (in the order of increasing off-orientation angle).

In particular, in the (110)perovskite films with a variant structure, the tunnelling magnetoresistance increases on passing from (001)$ZrO_2(Y_2O_3)$ to (111)$ZrO_2(Y_2O_3)$.

Tunnelling structures are often designed using epitaxial films of manganites on bicrystalline perovskite substrates. The films are grown on a special boundary produced, for example, by diffusion welding of two halves of a single-crystalline substrate. The structure of this boundary is inherited by the epitaxial film. Obviously, for practical application, multivariant structures on single-crystalline substrates have essential advantages over monovariant epitaxial structures on bicrystalline substrates. First, they are much less expensive and second, the whole surface of a variant film rather than only the bicrystalline boundary region can be used for the preparation of magnetic sensors.

Our further research has demonstrated that the field sensitivity of the variant structures based on manganite films can be increased through deposition of a layer of a soft ferromagnet (based on $MnFe_2O_4$) on a layer of the variant structure formed on the (111)$ZrO_2(Y_2O_3)$ substrate (Fig. 24, *cf.* curves *3*, *4* and *5*, *6*).

The variant structures also appear in films with other types of epitaxial interface. For example, a study of an In_2O_3 film (bixbyite cubic structure, $a = 1.0117$ nm) on (001)MgO (NaCl type, $a = 0.4213$ nm)[120] has shown that domains with the (111)In_2O_3 ‖ (001)MgO orientation, which split into four variant structures in the substrate plane, predominate in these films. In all of these structures, the diagonals of the cube faces of In_2O_3 and MgO are parallel: $[1\bar{1}0]In_2O_3$ ‖ [110]MgO, $[\bar{1}10]In_2O_3$ ‖ [110]MgO, $[110]In_2O_3$ ‖ $[1\bar{1}0]$MgO and $[110]In_2O_3$ ‖ $[\bar{1}10]$MgO. The same type of variant structure is typical of isostructural Y_2O_3 films on (001)MgO (Fig. 25 *a*).[121, 122] In both films (In_2O_3 and Y_2O_3), some of the crystallites are oriented with the (001) axis normal to the substrate; these crystallites are monovariant (Fig. 25 *b*). The ratio of the (111)- and (001)-oriented domains depends on the film deposition temperature and on the oxygen pressure in the evaporation chamber,[123] although the role of the latter is not quite clear. Probably, oxygen influences the rate of film deposition, which often switches the (111)-growth to the (001)-growth for cubic crystals. The formation of the variant structures has an essential influence on the conductivity of In_2O_3 films, because high-angle boundaries of the domains create additional resistance to the carrier transport. This circumstance should be taken into account when using In_2O_3 as a conductive layer on single-crystalline substrates.

Now we consider the growth of films with a rutile structure (TiO_2, CrO_2, RuO_2, SnO_2) on substrates of the fluorite and perovskite type. The length of the diagonal of the tetragonal face in the RuO_2 structure is close to the length of the edge of the fluorite cube [in $ZrO_2(Y_2O_3)$ and CeO_2] and to the length of the face diagonal of the perovskite cube [in $LaAlO_3$].[123] The orientation of the (100)RuO_2 ‖ (001)substrate film gives rise to four epitaxial modes of the growth (Fig. 26). In the RuO_2 film on *a*-sapphire, the (100)RuO_2 ‖ (0001)substrate orientation gives rise to three growth patterns with a common motif at the interface, $[010]RuO_2 \parallel [11\bar{2}0]Al_2O_3$, $[010]RuO_2 \parallel [\bar{2}110]Al_2O_3$ and $[010]RuO_2 \parallel [1\bar{2}10]Al_2O_3$.[124] It is noteworthy that the same film orientation takes place in the growth of rutiles on *R*-sapphire; however, the *R* plane has only one vector of the $[1\bar{2}10]Al_2O_3$ type; therefore, the epitaxy is monovariant: $(101)[010]MO_2 \parallel (\bar{1}012)[1\bar{2}10]Al_2O_3$.

The variant structures in the CrO_2 films with the rutile structure, as those in the manganites described above, show the tunnelling magnetoresistance effects, although they are weaker in magnitude.[125]

It follows from the foregoing that the variant structures (with high-angle domain boundaries) are actually heteroepitaxial nanostructures resulting from self-assembly on the substrate surface occurring in particular orientational relations with the growing film. They are to be distinguished from the mosaic single crystals in which the low-angle domain structures predominate and no rigid restrictions on the mutual orientation angle are involved.

Meanwhile, the variant structures have common features with single-crystalline twins. Whereas the prediction of a twin structure requires only crystal parameters, a variant epitaxial structure can be determined only with known crystallographic data for the film and the substrate and their epitaxial relations. Only in rare cases, does a variant structure correspond to twins known for this

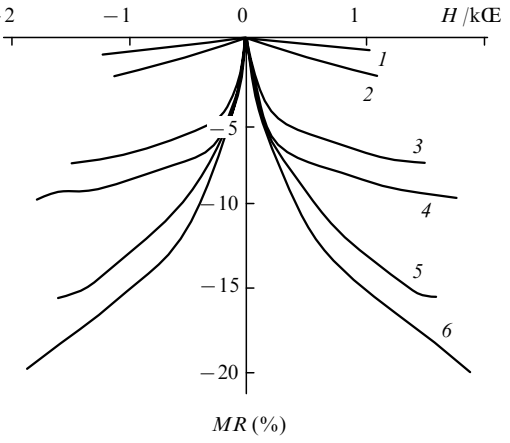


Figure 24. Magnetoresistance $MR = \{[R(H) - R(0)]/R(0)\} \cdot 100\%$ of films and heterostructures on different substrates.
(*1*) $(La_{0.7}Sr_{0.3})MnO_3$/MgO, (*2*) $(La_{0.7}Sr_{0.3})MnO_3$/(001)$SrTiO_3$, (*3*) $(La_{0.7}Sr_{0.3})MnO_3$/(110)$ZrO_2(Y_2O_3)$, (*4*) $MnFe_2O_4$/$(La_{0.7}Sr_{0.3})MnO_3$/(110)$ZrO_2(Y_2O_3)$, (*5*) $(La_{0.7}Sr_{0.3})MnO_3$/(111)$ZrO_2(Y_2O_3)$, (*6*) $MnFe_2O_4$/$(La_{0.7}Sr_{0.3})MnO_3$/(111)$ZrO_2(Y_2O_3)$.

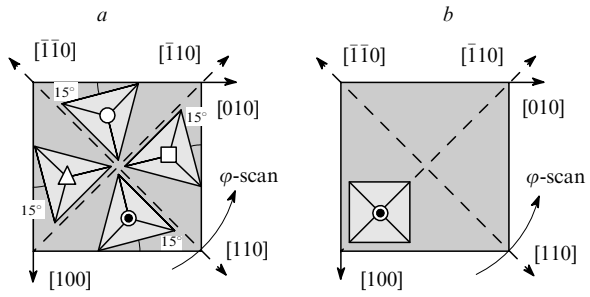


Figure 25. Modes of the epitaxial growth of Y_2O_3 on (001)MgO.[121, 122]
(*a*) Four modes of the growth of (111) domains, (*b*) monovariant growth of the (001) domains.

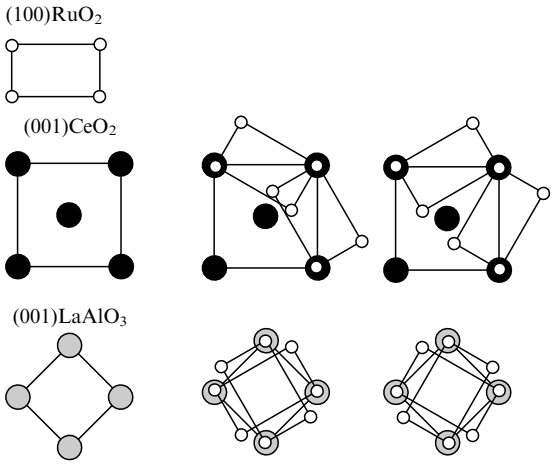


Figure 26. Four modes of the RuO_2 growth on the (001)CeO_2 fluorite and (001)$LaAlO_3$ perovskite.

crystal. This is usually the case for systems where the number of variants is reduced due to coincidence of some additional symmetry elements, as in *a*-oriented structures of $RBa_2Cu_3O_{7-\delta}$ related to each other by the (013) twinning plane.

It has been noted above that many perovskites tend to grow in the (110) orientation on fluorite substrates, for example, on $(001)ZrO_2(Y_2O_3)$. However, there are some exceptions. The $BaTiO_3$ epitaxial films have the (111) orientation on this substrate, which implies four epitaxial growth modes with a common motif: the length of the face diagonal of the perovskite cube is close to the length of the edge of the fluorite cube. These conditions are violated upon the change in the ratio of the lattice parameters of the film and the substrate. For example, deposition of $BaTiO_3$ on a buffer layer of the cubic praseodymium oxide (with the lattice parameter $a = 0.546$ nm) results in switching of the orientation of the $BaTiO_3$ film to (001), which provides the least misfit between the CSL parameters and the (001) layer of praseodymium oxide.[126]

Of considerable interest is further research into the kinetics of formation of variant structures and the possibility of controlling the nanodomain size, shape and arrangement on the substrate surface. The experimental data available to date attest to a dependence of the nanodomain size on the diffusive mobility of the film components. This in the MOCVD deposition of the $RBa_2Cu_3O_{7-\delta}$ films under conditions where the figurative point of the crystallising system occurs near the solidus surface, the domains of variant structures can grow to submicron dimensions. Some published data may be indicative of the possibility of controlling the shape anisotropy of the variant nanodomains. For the three-variant $(100)RuO_2$ structure on $(0001)Al_2O_3$, the following correlation was established: nanodomains with an average size of 30 nm are most extended along the direction of the least misfit of the CSL and least extended along the greatest misfit of the CSL. If this dependence is general, this would allow effective control of the shape of nanodomains through a change in the substrate material (and, hence, the parameter *a* of the substrate) by doping or deposition of buffer layers. The question concerning the possibility of fixing the arrangement of epitaxial variant structures on the substrate surface remains open. Apparently, interesting results could be provided by using vicinal or single-crystalline substrates with an artificial relief (graphoepitaxy).

Generally, variant structures represent a new group of thin-film materials whose physical properties (including electrical and magnetic ones) are determined at the nano-size level and differ appreciably from the properties of both monovariant epitaxial films and polycrystalline materials. Further research into these structures will promote extension of the scope of their application in the modern micro- and nanoelectronics.

IV. Conclusion

We would like to emphasise once again that the epitaxial stabilisation of oxide films discussed in this review is an equilibrium phenomenon, *i.e.*, the growing oxide phase exists in an external equilibrium with the substrate and the gas-phase oxygen and also in an internal (in the case of phase assembly) solid-state equilibrium. If the decrease in the Gibbs energy of the film/substrate system caused by epitaxy is greater in magnitude than the ΔG value of any solid-state process involving the phase growing on a substrate surface (a polymorphic transition, redox reaction, *etc.*), one can expect that phase equilibria in an epitaxial film would differ from the phase equilibrium in the same system without epitaxy. In particular, with epitaxial stabilisation, the 'unusual' simple or complex oxide phases that require high pressure, high temperature or high oxygen pressures to be formed can be prepared without resorting to these extrem conditions. In multiple phase films, the epitaxial relations of separate phases with the matrix phase in whose bulk they grow and/or with the substrate can give rise to stable phase assemblies differing from those dictated by the equilibrium phase diagram. All these phenomena can be regarded as being due to the change in the thermodynamics of the system under the action of epitaxy rather than to manifestation of slow kinetics of the surface reaction, which precludes attainment of the Gibbs energy minimum during the film growth. The effect of epitaxy on the thermodynamics of the growing phase is enhanced with an increase in the coherence of the film structure and the substrate. In the case of a perfect fit of the structures, the critical thickness of the stabilised phase reaches a maximum value.

This review considers examples of ES, taken mainly from our studies on gas-phase epitaxy; however, the ES phenomena are equally typical of the liquid-phase epitaxy (from aqueous solutions and melts), electrocrystallisation,§ and, perhaps, solid-state epitaxy. Moreover, the ES can be detected not only in the preparation of thin films or in the solid-state chemistry, but also in mineralogy (examples of pseudomorphism in minerals are frequently encountered [128]).

The understanding of the nature of the ES attained to date allows one to use this phenomenon for deliberate synthesis of unstable compounds as thin epitaxial films, which can soundly be expected to be a success. The films of epitaxially stabilised phases are of considerable interest not only as objects for the study of the fundamental properties of materials but also as real materials with potentially useful properties. The selective epitaxy based on the ES can find application in the preparation of complex heterostructures. It is beyond doubt that involving new types of single crystalline substrates in the practice of epitaxial stabilisation would give rise to new oxide compounds and materials.

The variant epitaxial structures have not yet received adequate attention. Meanwhile, they represent a new class of nanostructures in which self-assembly of nanodomains is due to the energetic degeneracy of various geometric modes of epitaxy. By conscious selection of substrates, one can change the number and the mutual orientation of epitaxial variant structures in the film. The considered examples of enhancement of the magnetoresistance in the doped lanthanum manganite films represent the first achievements made owing to the targeted design of high-angle boundaries of the epitaxial variant structures. Even now, one can state that this approach would diversify and, in some cases, markedly enhance the properties of materials (magnetic, electric, including ferroelectric, and optical properties) depending on the structure of internal interfaces.

In conclusion, the authors are happy to thank the colleagues who actively participated in various stages of the research covered in this review: Drs. I E Graboi, S V Samoilewnkov, M A Novozhilov and A A Bosak and students S Antonov, A Mikhailov and O Boitsova for their inestimable contribution to the experiments.

This work was carried out with partial financing by the Russian Foundation for Basic Research (Project Nos 02-03-33258 and 04-03-32505), the Volkswagen Stiftung (Grant I/77821) and the NWO Program of the Russia – Holland cooperation.

References

1. P D Dankov *Dokl. Akad. Nauk SSSR* **24** 773 (1939)
2. P D Dankov *Zh. Fiz. Khim.* **23** 1025 (1949)
3. F C Frank, J H van der Merwe *Proc. R. Soc. London, Ser. A* **198** 205 (1949)
4. J H van der Merwe *J. Appl. Phys.* **34** 117 (1963)
5. S Chen, M G Mason, H J Gysling, G R Paz-Pujalt, T N Blanton, T Castro, K M Chen, C P Fictorie, W L Gladfelter, A Franciosi, P I Cohen, J F Evans *J. Vac. Sci. Technol. A* **11** 2419 (1993)

§ The deposition of metals at potentials lower than the thermodynamic deposition potential [127] is apparently closely related to the ES.

6. S Tokita, N Tanaka, H Saitoh *Jpn. J. Appl. Phys.* **39** L169 (2000)
7. G S Herman, Y Gao *Thin Solid Films* **397** 157 (2001)
8. W Sugimura, A Yamazaki, H Shigetani, J Tanaka, T Mitsuhashi *Jpn. J. Appl. Phys.* **36** 7358 (1997)
9. C K Ong, S J Wang *Appl. Surf. Sci.* **185** 47 (2001)
10. M Murakami, Y Matsumoto, K Nakajima, T Makino, Y Segawa, T Chikyow, P Ahmet, M Kawasaki, H Koinuma *Appl. Phys. Lett.* **78** 2664 (2001)
11. B H Park, L S Li, B J Gibbons, J Y Huang, Q X Jia *Appl. Phys. Lett.* **79** 2797 (2001)
12. A B M A Ashrafi, A Ueta, A Avramescu, H Kumano, I Suemune, Y-W Ok, T-Y Seong *Appl. Phys. Lett.* **76** 550 (2000)
13. O Yu Gorbenko, I E Graboy, V A Amelichev, A A Bosak, A R Kaul, B Güttler, V L Svetchnikov, H W Zandbergen *Solid State Commun.* **124** 15 (2002)
14. L J LeGore, O D Greenwood, J W Paulus, D J Frankel, R J Lad *J. Vac. Sci. Technol., A* **15** 1223 (1997)
15. Y Gao, Y J Kim, S Thevuthasan, S A Chambers, P Lubitz *J. Appl. Phys.* **81** 3253 (1997)
16. N Fukushima, K Sano, T Schimizu, K Abe, S Komatsu *Appl. Phys. Lett.* **73** 1200 (1998)
17. N Fukushima, K Sano, T Schimizu, K Abe, S Komatsu *Mater. Res. Soc. Symp. Proc.* **494** 35 (1998)
18. H-M Christen, L A Boatner, J D Budai, M F Chisholm, L A Gea, D P Norton, C Gerber *Appl. Phys. Lett.* **70** 2147 (1997)
19. M N Khan, H-T Kim, T Kusawake, H Kudo, K Ohshima, H Uwe *J. Appl. Phys.* **86** 2307 (1999)
20. H B Liao, R F Xiao, P Yu, G K L Wong, J Q Zheng *J. Vac. Sci. Technol., A* **14** 2651 (1996)
21. L H Hamedi, N Lemee, M Guilloux-Viry, A Perrin, in *The 7th European Conference on Solid State Chemistry (Abstracts of Reports), Madrid, 1999* Vol. 1, p. 77
22. N Adachi, V P Denysenkov, S I Khartsev, A M Grishin, T Okuda *J. Appl. Phys.* **88** 2734 (2000)
23. T Okuda, T Katayama, H Kobayashi, N Kobayashi *J. Appl. Phys.* **67** 4944 (1990)
24. A Thavendrarajah, M Pardavi-Horvath, P E Wigen, M Gomi *IEEE Trans. Magn.* **25** 4015 (1989)
25. S Mino, M Matsuoka, A Tate, A Shibukawa, K Ono *Jpn. J. Appl. Phys.* **31** 1786 (1992)
26. M Y Chern, J -S Liaw *Jpn. J. Appl. Phys.* **36** 1049 (1997)
27. N Watanabe, N Takahashi, K Tsushima *Mater. Chem. Phys.* **54** 173 (1998)
28. Y Jia, M A Zurbuchen, S Wozniak, A H Carim, D G Schlom, L-N Zou, S Briczinski, Y Liu *Appl. Phys. Lett.* **74** 3830 (1999)
29. P G Ivanov, S M Watts, D M Lind *J. Appl. Phys.* **89** 1035 (2001)
30. F Y Yang, C L Chien, E F Ferrari, X W Li, G Xiao, A Gupta *Appl. Phys. Lett.* **77** 286 (2000)
31. X W Li, A Gupta, T R McGuire, P R Duncombe, G Xiao *J. Appl. Phys.* **85** 5585 (1999)
32. X W Li, A Gupta, G Xiao *Appl. Phys. Lett.* **75** 713 (1999)
33. A Gupta, X W Li, S Guha, G Xiao *Appl. Phys. Lett.* **75** 2996 (1999)
34. K Suzuki, P M Tedrow *Solid State Commun.* **107** 583 (1998)
35. R G Egdell, E Brand, D Kellett *J. Mater. Chem.* **9** 2717 (1999)
36. W Neubeck, L Ranno, M B Hunt, C Vettier, D Givord *Appl. Surf. Sci.* **139** 195 (1999)
37. T Fujii, M Takano, R Katano, Y Bando, Y Isozumi *J. Appl. Phys.* **66** 3168 (1989)
38. T Fujii, M Takano, R Katano, Y Bando, Y Isozumi *J. Cryst. Growth* **99** 606 (1990)
39. M Takano, T Fujii, Y Bando, in *New Functionality Materials, C, Synthetic Process and Control of Functionality Materials* (Eds T Tsuruta, M Doyama, M Seno) (Amsterdam: Elsevier, 1993) p. 745
40. Y Gao, Y J Kim, S A Chambers, G Bai *J. Vac. Sci. Technol., A* **15** 332 (1997)
41. D M Lind, S D Berry, G Chern, H Mathias, L R Testardi *J. Appl. Phys.* **70** 6218 (1991)
42. D M Lind, S D Berry, G Chern, H Mathias, L R Testardi *Phys. Rev. B* **45** 1838 (1992)
43. D M Lind, S P Tay, S D Berry, J A Borchers, R W Erwin *J. Appl. Phys.* **73** 6886 (1993)
44. F C Voogt, T Hibma, P J M Smulders, L Niesen *J. Cryst. Growth* **174** 440 (1997)
45. Y Gao, Y J Kim, S A Chambers *J. Mater. Res.* **13** 2003 (1998)
46. F C Voogt, T Fujii, P J M Smulders, L Niesen, M A James, T Hibma *Phys. Rev. B* **60** 11 193 (1999)
47. A Gupta, B W Hussey, A M Guloy, T M Shaw, R F Saraf, J F Bringley, B A Scott *J. Solid State Chem.* **108** 202 (1994)
48. V M Ievlev, A V Bulgakov, V I Trofimov, in *Rost i Substruktura Kondensirovannykh Plenok* (Growth and Substructure of Condensed Films) (Voronezh: Voronezh State University, 2000) p. 20
49. S Little, A Zangwill *Phys. Rev. B* **49** 16 659 (1994)
50. A P Sutton, R W Balluffi *Interfaces in Crystalline Materials* (Oxford: Calendron Press, 1995)
51. I Barin *Thermochemical Data of Pure Substances* Pt. 2 (Weinheim: VCH, 1989)
52. R C West (Ed.) *Handbook of Chemistry and Physics* (Boca Raton, FL: CRC Press, 1986)
53. S V Samoylenkov, O Yu Gorbenko, I E Graboy, A R Kaul, O Stadel, G Wahl, H W Zandbergen *J. Phys. IV* **9** 621 (1999)
54. B Schulte, M Maul, P Häussler, H Adrian *Appl. Phys. Lett.* **62** 633 (1993)
55. Y Q Li, J Zhao, C S Chern *Physica C* **195** 161 (1992)
56. S V Samoylenkov, O Yu Gorbenko, A R Kaul, A R Kuzhakhmetov, S A Zhgoon, G Wahl *Non-Linear Electromagn. Syst.* **13** 87 (1998)
57. O Yu Gorbenko, I E Graboy, A R Kaul, H W Zandbergen *J. Magn. Magn. Mater.* **211** 97 (2000)
58. O Yu Gorbenko, A R Kaul, A A Molodyk, V N Fuflyigin, M A Novozhilov, A A Bosak, U Krause, G Wahl *J. Alloys Compd.* **251** 337 (1997)
59. A A Molodyk, M A Novozhilov, I E Graboy, O Yu Gorbenko, I E Korsakov, A R Kaul *Electrochem. Soc. Proc.* **97** 1152 (1997)
60. A R Kaul, B V Seleznev *J. Phys. IV* **3** 375 (1993)
61. H L Yakel, W C Kohler, E F Bertaut, E F Forrat *Acta Crystallogr.* **16** 957 (1963)
62. A Waintal, J Chenavas *Mater. Res. Bull.* **2** 819 (1967)
63. G Szabo Ph.D. Thesis, University of Lyon, Lyon, 1969
64. A A Bosak, A A Kamenev, I E Graboy, S V Antonov, O Yu Gorbenko, A R Kaul, C Dubourdieu, J P Senateur, V L Svechnikov, H W Zandbergen, B Hollaender *Thin Solid Films* **400** 149 (2001)
65. P A Salvador, T D Doan, B Mercey, B Raveau *Chem. Mater.* **10** 2592 (1998)
66. N Fujimura, T Ishida, T Yoshimura, T Ito *Appl. Phys. Lett.* **69** 1011 (1996)
67. A A Bosak, C Dubourdieu, J-P Sénateur, O Yu Gorbenko, A R Kaul *J. Mater. Chem.* **12** 800 (2002)
68. T Atsumi, T Ohgushi, N Kamegashira *J. Alloys Compd.* **238** 35 (1996)
69. A A Bossak, I E Graboy, O Yu Gorbenko, A R Kaul, M S Kartavtseva, V L Svetchnikov, H W Zandbergen *Chem. Mater.* **16** 1751 (2004)
70. P Lacorre, J B Torrance, J Pannetier, A I Nazzal, P W Wang, T C Huang *J. Solid State Chem.* **91** 225 (1991)
71. M A Novojilov, O Yu Gorbenko, I E Graboy, A R Kaul, H W Zandbergen, N A Babushkina, L M Belova *Appl. Phys. Lett.* **76** 2041 (2000)
72. Yu D Tretyakov, A R Kaul, V K Portnoy *High Temp. Sci.* **9** 61 (1977)
73. Y Kanke, A Navrotsky *J. Solid State Chem.* **141** 424 (1998)
74. O Yu Gorbenko, M A Novojilov, I E Graboy, V A Amelichev, A A Bosak, I V Nikulin, A R Kaul, B Guettler, G Wahl, N A Babushkina, L M Belova, H W Zandbergen *Int. J. Inorg. Mater.* **3** 1303 (2001)
75. G Demazeau, M Pouchard, P Hagenmuller *C. R. Acad. Sci., Ser. C* **277** 107 (1973)
76. A Yu Kropanev, A N Petrov *J. Inorg. Chem.* **28** 1667 (1983)
77. M A Novojilov, G E Adamov, A R Kaul, I E Graboy, H W Zandbergen, in *Processes for Micro- and Nanotechnologies (Proceedings of NATO ASI Series), Kaunas, 2001* p. 20
78. N V Porotnikov, O I Kondratov, K I Petrov, O V Sidorova *Zh. Neorg. Khim.* **25** 3224 (1980)[a]

79. C W F T Pistorius, G J Kruger *J. Inorg. Nucl. Chem.* **38** 1471 (1976)
80. K I Portnoi, N I Timofeeva *Kislorodnye Soedineniya Redkozemel'nykh Elementov* (Oxygen Compounds of Rare Earth Elements) (Moscow: Metallurgiya, 1986)
81. V A Amelitchev, M A Novojilov, O Yu Gorbenko, A R Kaul, B Güttler, in *Thin Films Depositions of Oxide Multilayers (Industrial-Scale Processings)* (Vilnius: Vilnius University Press, 2000) p. 91
82. O Yu Gorbenko, I E Graboy, M A Novozhilov, A R Kaul, G Wahl, V L Svetchnikov *J. Phys. IV* **11** 247 (2001)
83. J A M van Roosmalen, P van Vlaanderen, E H P Cordfunke, W L IJdo, D J W IJdo *J. Solid State Chem.* **114** 516 (1995)
84. B Bochu, J Chenavas, J C Joubert, M Marezio *J. Solid State Chem.* **11** 88 (1974)
85. J F Sarver, F L Katnack, F A Hummel *J. Electrochem. Soc.* **106** 960 (1959)
86. A Ohtomo, M Kawasaki, T Koida, M Masubuchi, H Koinuma, Y Sakurai, Y Yoshida, T Yasuda, Y Segawa *Appl. Phys. Lett.* **72** 2466 (1998)
87. Y Matsumoto, M Murakami, Z W Jin, A Ohtomo, M Lippmaa, M Kawasaki, H Koinuma *Jpn. J. Appl. Phys.* **68** L603 (1999)
88. A Ohtomo, R Shiroki, I Ohkubo, H Koinuma, M Kawasaki *Appl. Phys. Lett.* **75** 4088 (1999)
89. A K Sharma, J Narayan, J F Muth, C W Teng, C Jin, A Kvit, R M Kolbas, O W Holland *Appl. Phys. Lett.* **75** 3327 (1999)
90. E Millon, O Albert, J C Loulergue, J Etchepare, D Hulin, W Seiler, J Perriere *J. Appl. Phys.* **88** 6937 (2000)
91. T Fukumura, Z Jin, A Ohtomo, H Koinuma, M Kawasaki *Appl. Phys. Lett.* **75** 3366 (1999)
92. C H Bates, W B White, R Roy *J. Inorg. Nucl. Chem.* **28** 397 (1966)
93. C L Chang, G Chern, C L Chen, H H Hsieh, C L Dong, W F Pong, C H Chao, H C Chien, S L Chang *Solid State Commun.* **109** 599 (1999)
94. P C Donahue, L Katz, R Ward *Inorg. Chem.* **5** 335 (1966)
95. H W Zandbergen, E Connolly, I E Graboy, V L Svetchnikov, A R Kaul *Physica C* **329** 37 (2000)
96. K Fröhlich, J Šouc, A Rosová, D Machajdik, I E Graboy, V L Svetchnikov, A Figueras, F Weiss *Supercond. Sci. Technol.* **10** 657 (1997)
97. I E Korsakov, Candidate Thesis in Chemical Sciences, Moscow State University, Moscow, 1993
98. G F Voronin, in *Materials and Crystallographic Aspects of T_c Superconductivity (Proceedings of NATO ASI Series), Erice, Italy, 1993* p. 194
99. H Grimmer *Acta Crystallogr.* **32** 783 (1976)
100. B K Vanshtein, A A Chernov, L A Shuvalov (Eds) *Sovremennaya Kristallografiya* (Modern Crystallography) (Moscow: Nauka, 1980)
101. V M Kosevich, V M Ievlev, L S Palatnik, A I Fedorenko *Struktura Mezhkristallitnykh i Mezhfaznykh Granits* (Structure of Intergrain Boundaries and Interfaces) (Moscow: Metallurgiya, 1980)
102. A Somorjia, in *Introduction to Surface Chemistry and Catalysis.* (New York: Wiley, 1994) p. 667
103. H Nagata, T Tsukahara, S Gonda, M Yoshimoto, H Koinuma *Jpn. J. Appl. Phys.* **30** L1136 (1991)
104. A A Bosak, A N Botev, O Yu Gorbenko, I E Graboy, S V Samoylenkov, A R Kaul, C Dubordieu, J P Senateur *J. Phys. IV* **11** 93 (2001)
105. Y Y Erokhin, O Yu Gorbenko, I E Graboy, A R Kaul, S Pozigun, W Decker, R Stolle, G Wahl, in *Proceedings of the VIth Trilateral German-Russian-Ukrainian Seminar on HTSC, Dubna, 1994* p. 407
106. S V Samoylenkov, O Yu Gorbenko, A R Kaul, S V Papucha, N A Mirin, V V Maleev, I E Graboy, in *Proceedings of the XIVth International Conference on CVD and EUROCVD-XI, Paris, 1997* Vol. 97-25, p. 990
107. C V Samoilenkov, O Yu Gorbenko, A R Kaul, I E Graboy, S A Zhgun, in *Materialy X Mezhdunarodnogo Simpoziuma 'Tonkie Plenki v Elektronike', Yaroslavl', 1999* (Proceedings of the Xth International Symposium 'Thin Films in Electronics', Yaroslavl', 1999) p. 65
108. T Hashimoto, M Sagoi, Y Mizutani, J Yoshida, K Mizushima *Appl. Phys. Lett.* **60** 1757 (1992)
109. Z Trajanovic, C J Lobb, M Rajeswari, I Takeuchi, C Kwon, T Venkatesan *Phys. Rev. B* **56** 925 (1997)
110. O Yu Gorbenko, A R Kaul, A A Bosak, I E Graboy, H W Zandbergen, V L Svetchnikov, N A Babushkina, L M Belova, K I Kugel *Solid State Commun.* **114** 407 (2000)
111. S Y Hou, J Kwo, R K Watts, J-Y Cheng, D K Fork *Appl. Phys. Lett.* **67** 1387 (1995)
112. H N Lee, S Senz, A Visinoiu, A Pingolet, D Hesse, U Gosele *Appl. Phys., A: Mater. Sci. Process* **71** 101 (2000)
113. H N Lee, D Hesse, N Zakharov, U Gosele *Science* **296** 2006 (2002)
114. D Hesse, S K Lee, X H Zhu, N Zakharov, H N Lee, in *The 14th International Conference on Crystal Growth in Conjunction with the 12th International Conference on Vapour Growth and Epitaxy (Book of Abstracts), Grenoble, 2004* p. 395
115. O Yu Gorbenko, A A Bosak *Sensor* **1** (2) 28 (2002)
116. K Steenbeck, T Eick, K Kirsch, K O'Donnell, E Steinbeiß *Appl. Phys. Lett.* **71** 968 (1997)
117. C Dubourdieu, M Audier, H Roussel, J P Sénateur, J Pierre *J. Appl. Phys.* **92** 379 (2002)
118. K-K Choi, T Taniyama, Y Yamazaki *J. Appl. Phys.* **90** 6145 (2001)
119. S P Isaac, N D Mathur, J E Evetts, M G Blamire *Appl. Phys. Lett.* **72** 2038 (1998)
120. H Sieber, S Senz, D Hesse *Thin Solid Films* **303** 216 (1997)
121. R J Gaboriaud, F Pailloux, J Pacaud, P O Renault, J Perriere, A Huignard *Appl. Phys., A: Mater. Sci. Process* **71** 675 (2000)
122. R J Gaboriaud, F Paumier, F Pailloux, P Guerin *Mater. Sci. Eng. B* **109** 34 (2004)
123. Q X Jia, X D Wu, G Song, S R Foltyn *J. Vac. Sci. Technol., A* **14** 1107 (1996)
124. Q Wang, W L Gladfelter, D F Evans, Y Fan, A Franciosi *J. Vac. Sci. Technol., A* **14** 747 (1996)
125. U Rüdiger, M Rabe, K Samm, B Özyilmaz, J Pommer, M Fraune, G Güntherodt, S Senz, D Hesse *J. Appl. Phys.* **89** 7699 (2001)
126. O Yu Gorbenko, A R Kaul, G Wahl *Chem. Vap. Depos.* **3** 193 (1997)
127. L J Buller, H D Abruna *Chem. Rev.* **101** 1897 (2001)
128. V S Urusov, V L Tauson, V V Akimov *Geokhimiya Tverdogo Tela* (Geochemistry of Solids) (Moscow: GEOS, 1997)

[a] — *Russ. J. Inorg. Chem. (Engl. Transl.)*